NASA

MEMORANDUM

AERODYNAMIC CHARACTERISTICS OF SOME FAMILIES

OF BLUNT BODIES AT TRANSONIC SPEEDS

By Lewis R. Fisher, Arvid L. Keith, Jr.,
and Joseph R. DiCamillo

Langley Research Center
Langley Field, Va.

[redacted]

NATIONAL AERONAUTICS AND SPACE ADMINISTRATION

WASHINGTON

November 1958

Code!

copy #1

NATIONAL AERONAUTICS AND SPACE ADMINISTRATION

NASA MEMO 10-28-58L

AERODYNAMIC CHARACTERISTICS OF SOME FAMILIES OF BLUNT BODIES AT TRANSONIC SPEEDS*

By Lewis R. Fisher, Arvid L. Keith, Jr.,
and Joseph R. DiCamillo

SUMMARY

Several families of blunt bodies having shapes that may be applicable to atmospheric reentry bodies were tested to determine the lift, drag, and pitching-moment characteristics at transonic speeds for Reynolds numbers between 2.4 and 6.0 million.

The entire series of bodies was statically stable with the stability being highest for those models with a large amount of surface area behind the moment reference point. For such shapes, the amount of stability depended upon where the flow which was separated at the body shoulders was able to become reattached to the body. The lift-curve slope was generally positive for bodies which increased in diameter in the downstream direction and negative for those with an opposite slope.

The deflection of a control wedge on the rear portion of a blunt body altered the trim lift coefficients appreciably, without, however, materially affecting the stability. Body indentation increased the static stability substantially provided that the flared portion of the skirt extended well into the airstream.

INTRODUCTION

Blunt shapes have been shown in reference 1 to be more suitable for atmospheric reentry bodies than sharp-nose shapes because of the significantly lower convective-heat-transfer rates in the region of the stagnation point and because of the dispersion of energy through the strong bow shock associated with the blunt shape. In addition to the solution of the aerodynamic heating problem, a second requirement for satisfactory and successful reentry is that the missile have sufficient dynamic stability to damp any oscillation that may occur during its flight.

*Title, Unclassified.

Because reentry bodies may be designed to decelerate to subsonic speeds before impact, aerodynamic data in the transonic speed regime is of interest for blunt shapes in order that assessment may be made of the relative importance of geometric parameters on their stability. In reference 2, the degree of dynamic stability is shown to be a function of the aerodynamic pitch damping, the lift-curve slope, and the drag; the degree of static stability is shown to be a function of the static-stability parameter and the lift-curve slope.

The purpose of the present tests, therefore, was to evaluate the effects of certain geometric parameters on the static aerodynamic coefficients at transonic speeds for several families of geometrically related blunt shapes which appear, from aerodynamic heating considerations, to be suitable as reentry bodies. The investigation was made in the Langley transonic blowdown tunnel for Mach numbers between 0.7 and 1.3 and at Reynolds numbers between 2.4 and 6.0×10^6 based on a body dimension of 3 inches.

SYMBOLS

The data are referred to the system of stability axes (fig. 1) and are presented in the form of standard coefficients of forces and moments about a point one-third of the length of the model rearward from the front face with the exception of the data for models 11 and 17 for which the moment reference points are specified. The coefficients and symbols used herein are defined as follows:

a length of skirt measured parallel to axis of symmetry from 0.1l

C_D drag coefficient, $\frac{\text{Drag}}{qS}$

C_{D_o} drag coefficient at zero lift

C_L lift coefficient, $\frac{\text{Lift}}{qS}$

C_m pitching-moment coefficient, $\frac{\text{Pitching moment}}{qSd}$

$C_{L_\alpha} = \frac{\partial C_L}{\partial \alpha}$, 1/radian

$C_{m_\alpha} = \frac{\partial C_m}{\partial \alpha}$, 1/radian

$C_{m_\delta} = \frac{\partial C_m}{\partial \delta}$, 1/radian

d	maximum diameter of model
l	length of model
M	free-stream Mach number
p_t	free-stream stagnation pressure
q	free-stream dynamic pressure, $\frac{1}{2}\rho V^2$
R	Reynolds number (based on a body dimension of 3 inches)
S	maximum cross-sectional area of model
V	free-stream velocity
x_{cp}	longitudinal distance from face of model to center of pressure, positive rearward
α	angle of attack
δ	angle of control-wedge deflection
ρ	mass density of air in free stream

The nomenclature of the blunt body is shown by the following sketch:

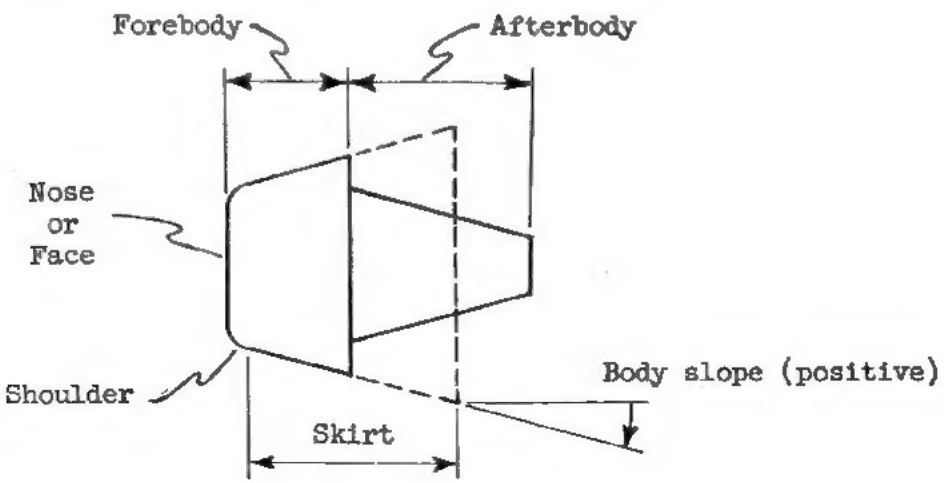

APPARATUS AND TESTS

Models.- The families of models tested are described by the sketches and photograph of figures 2 and 3. The models, which are designated numerically, are grouped in table I to show conveniently the family relationships. Certain basic models have variants which are designated by the basic-model number and a letter. The model families were designed in order to isolate the effects of such geometric parameters as skirt length, body slope, nose radius, shoulder radius, and body indentation on the aerodynamic characteristics. Models 1 to 5 vary only in skirt length. Models 7 to 10 vary in body slope, while models 7b and 9b differ from models 7 and 9, respectively, only in shoulder radius. The family of models 12 to 14 differ only in nose radius, and models 18 to 22 constitute the body-indentation series. Models 11 and 17 do not fit into any of these families but were included in the tests as representative shapes.

It may be noted that in most cases it is possible to cross-relate at least one geometric variable between the various groups. For example, models 3 and 13 vary only in the slope of the afterbody. Model 7 was tested with the addition of 15° and 30° wedges on the lower surface to simulate the deflection of a portion of the skirt as an aerodynamic control device. This model was also tested with a nose ring placed on the shoulder to insure airflow detachment. To insure the existance of a turbulent boundary layer, a strip of roughness 5/16 inch wide and composed of carborundum grains 0.001 to 0.002 inch in diameter (ref. 3) was installed on the shoulder of those models having a rounded shoulder.

Tests.- The models were sting-mounted in the Langley transonic blowdown tunnel which is described in reference 4. Axial and normal forces and pitching moment were obtained by means of a three-component strain-gage balance. The output of the balance was transferred to potentiometers and continuously recorded on strip charts. Tunnel Mach number, dynamic pressure, and unit Reynolds number were determined from film records obtained from continuously operating flight-type recorders. The test Mach number differed from a desired value by as much as 0.03 for the range of test conditions. This result was due to the fact that for the high-drag configurations investigated, the test Mach number depended upon such factors as model size, angle of attack, and shape, and for the lower Reynolds numbers, upon the skill of the tunnel operator in controlling the stagnation pressure. (See ref. 4.)

The tests were conducted at tunnel stagnation pressures of 35 and 70 psia, which correspond to a Reynolds number range, based on a 3-inch model dimension, of from 2.4 to 6.0×10^{6} for the test Mach number range (see fig. 4) from 0.7 to 1.3. All models were tested at angles of attack

from 0° to 8°. At the lower stagnation pressure, angles of attack up to 12° were obtained. The models with the deflected wedge control were also tested through negative angles of attack as low as -12°.

RESULTS AND DISCUSSION

Presentation of Results

For the presentation of the test results, the measured normal and axial forces were converted to lift and drag forces and are presented as lift and drag coefficients. The variations of the lift, drag, and pitching-moment coefficients with angle of attack for the several families of blunt bodies tested at transonic speeds are presented in figures 5 to 23. Included in these figures for certain families are the variations of the static-stability derivatives C_{L_α} and C_{m_α} with body geometry. The latter is employed as a qualitative variable in some instances. The aerodynamic coefficients C_{L_α}, C_{m_α}, and C_{D_o} are presented directly as functions of Mach number for six of the model families in figures 24 to 29, and figure 30 presents the movement of the longitudinal center of pressure with Mach number for these families. A comparison of some of the transonic data with values computed by means of hypersonic theory for one model is made in figure 31.

The aerodynamic coefficients presented for all the bodies tested are based on the maximum diameter of the body as the reference dimension in all basic data figures. However, in figures 24 and 29, in order to provide a basis for comparison which would not be disguised by differences in body diameter among models of the same family, the coefficients are based on a single reference diameter in each of these figures. The skirt-length and indented-body families (figs. 24 and 29, respectively) are the only families of models for which the model diameters vary.

Variations With Angle of Attack

The skirt-length family.- The effect of reducing the length of the skirt of a positively sloped body (a body whose diameter increases in the downstream direction is herein considered to have a positive slope) on the aerodynamic coefficients of the body is shown in figure 5 for the higher of the two ranges of Reynolds number at which tests were made. All dimensions for this family of shapes are the same with the exception of the length of the skirt and the maximum diameters. The coefficients presented in figure 5 are based on the actual maximum diameter for each model.

The lift-curve slope is shown in figure 5(a) to be positive for only the full skirt of model 1. The two shorter skirts of models 3 and 4 resulted in higher drag coefficients for these blunt bodies (fig. 5(b)) which were not entirely due to the decreasing area upon which the coefficients were based. The skirt length apparently influences the drag of the model by its effect on the base pressure behind the body. Model 1 with the longest skirt had more longitudinal stability (fig. 5(c)) than did the models with the shortened skirts. This reduction in stability is due to the loss of lift-producing surface area well behind the model center of gravity.

Figure 6 presents the effect of reducing the skirt length for a family of blunt shapes similar to that of figure 5 for the lower Reynolds number range and a slightly larger range of angle of attack. These results are similar to the higher Reynolds number data of figure 5. It is interesting to note that when the length of the skirt is reduced to a certain point, then a further reduction does not appear to have any further effect on either the lift or pitching moment. Certain of the models shown in figures 5 and 6, and in succeeding figures, were not tested at $\alpha = 0^\circ$. In these cases, all lift and pitching-moment curves were faired through zero at $\alpha = 0^\circ$.

The slopes C_{L_α} and C_{m_α} measured from the data of figures 5 and 6 are shown as functions of skirt length in figure 7. It may be noted that doubling the Reynolds number had no appreciable effect on the slopes for this series of models. The variation of these derivatives with Mach number is presented in figure 24.

The shoulder-radius family.- In figure 8 is shown the effect of a shoulder radius on the aerodynamic coefficients for a blunt body. Model 7b, which had a sharp-cornered shoulder was tested as an example of a shape which would have a tendency toward separation of the boundary layer in the shoulder region at least at subsonic speeds. Such separation may not be realized from a rounded-shoulder body such as model 7. Some effect of the shoulder radius on the lift and drag can be noted in figure 8, but the major effect appears to be on the pitching moment. For subsonic Mach numbers and for the lower Reynolds number range, the sharp-cornered model 7b had a greater value of C_{m_α} than the round-cornered model 7. This difference can be explained by a reattachment of the flow somewhere along the upper surface of the skirt of model 7 which results in a positive increment in pitching moment. In the case of the sharp-cornered model 7b, reattachment of the flow could not occur; hence, the more negative pitching moments. At the higher Mach numbers the flow is able to expand supersonically around the corner of model 7b with reattachment occurring and with the resulting higher pressures on the upper surface of the model tending to decrease the negative C_{m_α} and to decrease C_{L_α}. These effects are shown clearly in figure 25.

The results of figures 8 and 25 also indicate that a round-cornered body such as model 7 can have aerodynamic characteristics similar to a sharp-cornered body such as model 7b if the separation point is fixed by putting a nose ring on the model. Model 7 with a circular nose ring on the shoulder radius was tested as model 7a. The characteristics exhibited by model 7a are shown in figures 8 and 25 to be very similar to those for model 7b.

A Reynolds number effect is also apparent in figure 8(c). At $M = 1.0$, it appears that, at the lower Reynolds number, the flow was unattached for the sharp-cornered model 7b over the full range of angle of attack, whereas at the higher Reynolds number, the flow reattached for angles of attack less than 8°. At higher angles of attack, for the latter case, the angle became too great for supersonic expansion to take place and the flow could not reattach. For the highest Mach number, the flow was able to expand supersonically about the corner and the flow reattached at all angles of attack. These results might lead to the deduction that at still higher supersonic Mach numbers, the flow reattachment would take place at points successively farther upstream along the skirt with a consequent reduction in static stability with increasing Mach number. Some unpublished transonic test results (Ames Research Center) indicated that for blunt bodies similar to some of those tested herein, the longitudinal characteristics measured for increasing angles of attack differed significantly from the corresponding results measured for decreasing angles of attack. This effect, which was related to flow separation downstream of the shoulder, tended to show some dependence on Reynolds number. The existence of such an aerodynamic hysteresis effect could not be ascertained during the present tests because of the test procedure used.

In figure 9 is shown the effect of shoulder radius on the aerodynamic coefficients for a negatively sloped body. The lift-curve slope for the sharp-cornered model was more negative than that for the round-cornered model for all Mach numbers and both Reynolds numbers. The use of a sharp rather than rounded shoulder resulted in a considerable increase in the drag coefficients for the body but had no effect on the pitching-moment curves.

The body-slope family.- The effect of the slope of the body on the aerodynamic coefficients at the higher Reynolds numbers is shown in figure 10. Models 7 and 9 had a 10° slope, positive and negative, respectively, while model 8 had zero slope. Figure 10(a) indicates that the sign of the lift-curve slope is the same as the direction of the body slope; that is, a positively sloped body results in a positive lift-curve slope, and a negatively sloped body results in a negative lift-curve slope. This conclusion is borne out by the lift-curve slopes shown in figures 7 and 24 as well. The picture is not so clear-cut for model 8 with a cylindrical body. The lift-curve slope for this shape is negative at subsonic Mach numbers and positive at supersonic Mach

numbers. These results, with the aid of the results for models 7 and 9 in figure 10(a), can again be explained in terms of flow separation and reattachment. At supersonic Mach numbers, model 8 suffered a rather violent decrease in lift between angles of attack of 6° and 8° which is indicative of a flow separation between these angles of attack. These effects of body slope, and of Reynolds number on the lift forces for such bodies, are in general agreement with the results of reference 5 which describes low-speed tests of two-dimensional cylinders of varying cross-sectional shape.

The drag coefficient, figure 10(b), is apparently dependent to a large degree on the frontal surface area presented to the airstream. The Newtonian theory indicates that frontal surface area also determines the major part of the drag of blunt bodies at hypersonic speeds. The pitching-moment curves in figure 10(c) show a somewhat greater amount of static stability for model 8 than for the sloped-body models. At high Mach numbers, however, C_{m_α} for model 8 became positive at high angles of attack.

In figure 11 the data for the same family of models at the lower Reynolds numbers are presented together with an additional model with a body slope of -20°. In general, these results are the same as those for the higher Reynolds number data of figure 10. The further decrease in body slope of model 10 contributed practically nothing to the results shown for model 9.

The slopes C_{L_α} and C_{m_α} are presented directly as functions of body slope in figure 12 and of Mach number in figure 27. The dependence of C_{L_α} upon body slope is clearly shown in figure 12. Model 8 exhibits some rather strong effects of Reynolds number in this figure which indicate the criticallity of the flow about such a model.

The control-wedge family.- A family of bodies was formed by adding 15° and 30° wedges to the bottom surface of model 7 in order to simulate the deflection of a portion of the skirt as an aerodynamic control device. The aerodynamic coefficients for these models, shown in figures 13 and 14, indicate incremental lift, drag, and pitching-moment coefficients for all angles of attack from $\alpha = -12^\circ$ to $\alpha = 12^\circ$ with the slopes of the coefficients with angle of attack being generally the same for the three models. The 7-15 model reached a trim condition at an angle of attack between -2° and -6° depending upon Mach number, but the 7-30 model was not trimmed in the angle-of-attack range tested, although the pitching moment was only slightly negative at $\alpha = -12^\circ$. The value of C_{m_δ} for these models was roughly 0.2 per radian. Reynolds number had no apparent effect on these data. The discontinuities which appear in the drag data at the nominal Mach number $M = 1.0$ are due to

differences in the actual test Mach numbers between the negative and positive ranges of angle of attack.

The nose-curvature family.- The effect of nose curvature on the aerodynamic characteristics of a blunt body with a short skirt is presented for the high Reynolds number range in figure 15 and for the low Reynolds number range in figure 16; C_{L_α} and C_{m_α} are shown for both Reynolds number ranges in figure 17. The most negative lift-curve slopes were shown by the slightly curved face of model 13, whereas those for the hemispherical face of model 14 were about zero with Reynolds number having little effect for these two models. At the lower Reynolds numbers (fig. 16), the lift for the flat-faced model 12 fell in between the lift values for the other two models. At the higher Reynolds numbers (fig. 15), however, the lift curve for model 12 approximated that for model 13 at subsonic Mach numbers and that for model 14 at supersonic Mach numbers, except for the highest angle of attack. The slightly curved face of model 13 produced the highest drag at subsonic Mach numbers, but at supersonic speeds the drag tended to become approximately equal for all models. Nose curvature had no effect on the pitching-moment slopes for this type of model. From figure 17, it appears that the flat-faced model 12 exhibits the largest effects of Reynolds number on C_{L_α}.

The indented-body families.- A family of bodies was derived by indenting model 7 by equal amounts at two longitudinal locations along the body to provide skirt flare angles larger than that of the basic body. The effect of body indentation on the aerodynamic coefficients for this family of blunt bodies is shown in figure 18 for the high Reynolds number range and in figure 19 for the low Reynolds number range. Model 18, which had the forward indentation, had about the same lift-curve slopes as the basic model 7 but had higher drag and pitching-moment coefficients at all angles of attack with the static stability in pitch being increased by a factor of from 2 to 3. Model 19, with the rearward indentation, experienced a reduction in lift-curve slope over models 7 and 18 and showed somewhat higher drag and generally less stability than did model 18 with the forward indentation.

In figure 20 is presented the aerodynamic coefficients for another family of indented blunt bodies. The models of this family all have the same nose-surface areas; the coefficients again are based on the maximum diameter of each model. The results indicate that the indented bodies have lower lift-curve slopes than either of the flat-sided bodies, but at the same time, more static stability which is probably due to the aerodynamic loadings being concentrated toward the rear of the indented bodies. The coefficients for the cylindrical model 22 show the same sensitivity to Mach number as was shown by model 8 (fig. 10). The

derivatives C_{L_α} and C_{m_α} are presented in figure 21 for the entire series of indented bodies.

Miscellaneous models.- The aerodynamic coefficients for a flared, flat-faced cylinder at transonic speeds are shown in figure 22. At the lower Mach numbers, the model had positive lift-curve slopes and positive static stability, but at $M = 1.3$, the lift-curve slope was sharply reduced and the static stability went to about zero at low angles of attack with the pitching moment being measured at 30.3 percent of the model length. These trends of the lift and pitching moment are consistent with those observed for the previously discussed sharp-cornered model 7b in that at the highest Mach number the flow is able to expand about the upper shoulder making the upper surface of the flared portion effective in producing negative lift and positive pitching moment. At angles of attack higher than 4°, the flow is no longer able to accomplish the expansion, separation occurs, and the upper surface of the flare loses its effectiveness.

The aerodynamic coefficients at transonic speeds for a round-nose cone are presented in figure 23. The lift and pitching-moment curves (measured at 58 percent l) were about the same through the transonic range of Mach numbers.

Variations With Mach Number

In order to show directly the effects of Mach number in the transonic range on the aerodynamic characteristics of blunt bodies, the coefficients C_{m_α}, C_{L_α}, and C_{D_o} are presented in figures 24 through 29 as functions of Mach number. For those instances wherein a model was not tested at $\alpha = 0^\circ$, C_{D_o} in these figures represents the drag coefficient at $\alpha = 4^\circ$. All the coefficients presented in figures 24 and 29 are based on common model diameters which are those for model 1 and model 20, respectively.

It appears that the effect of Mach number on the aerodynamic characteristics is directly dependent upon the detailed model geometry. In general, the models which had the largest amount of skirt area exposed to the airstream showed the largest effects of Mach number on the static stability.

The variation of the center-of-pressure location with Mach number is shown in figure 30 for several families of blunt bodies. In computing the center-of-pressure location, the drag component of the pitching moment was taken into consideration so that the result, in effect, is a

resultant center of pressure. The relationship for the center of pressure is

$$\frac{x_{cp}}{l} = -\frac{C_{m_\alpha}}{C_{L_\alpha} + C_{D_o}} \frac{d}{l} + \frac{1}{3}$$

where x_{cp} is the distance measured rearward from the face of the model. The flow-reattachment process is shown by models 7 and 7b to induce a forward shift in the resultant center of pressure at subsonic speeds. The loadings are shifted toward the rear, however, by a large control wedge (models 7, 7-15, and 7-30) or by flaring the skirt (models 7, 18, and 19). A positive to negative alteration of the body slope causes a forward shift in the loadings (models 7, 9, and 10) although the cylindrical model 8 indicates that its center-of-pressure location is rather sensitive to Mach number. A substantial increase in both the nose-curvature (models 12, 13, and 14) or the skirt length (models 1 and 4) shifts the aerodynamic loadings rearward.

Comparison With Hypersonic Theory

A comparison of C_{L_α} and C_{D_o} at transonic speeds and at $M = 3$ for model 7b is made with values calculated from Newtonian impact theory in figure 31. The $M = 3$ test points are unpublished data measured on a geometrically similar model. The comparison in figure 31 is not intended to imply that transonic lift and drag coefficients for blunt bodies can be estimated from impact theory but rather to show that the trends of the higher transonic values and a low supersonic value appear to approach the hypersonic (impact theory) derivatives asymptotically. Jones' low-aspect-ratio-wing theory, although derived for thin wings, results in a value of C_{L_α} for a wing with a plan form the same as that of model 7b which closely approximates the subsonic test values for model 7b.

CONCLUSIONS

Several families of blunt bodies having shapes which may make them suitable for atmospheric reentry bodies were tested through the transonic speed range to determine their lift, drag, and pitching-moment characteristics at these speeds. The results of this investigation indicate the following conclusions:

1. The entire series of bodies was statically stable in pitch about a point one-third of the length of the body rearward from the face. The

degree of stability was greatest for those models with the largest amount of surface area behind the moment reference point such as a model with increasing diameter in the downstream direction would have. For this type of shape, the stability was higher for those models for which boundary-layer separation occurred over greater distances along the model skirt. The condition of flow reattachment was found to be governed by the shoulder radius of the model and by the Reynolds and Mach numbers of the airflow. The stability of a cylindrical model was found to be particularly sensitive to Reynolds number and Mach number.

2. In general the sign of the lift-curve slope was determined by the direction of the slope of the body sides; the slope was positive for bodies which increased in diameter in the downstream direction and negative for those with an opposite slope.

3. The trim lift coefficients were altered for a model without appreciably affecting the static stability by deflecting a control wedge on the rear portion of the skirt.

4. The face curvature of a short-skirted model determined the magnitude of the lift-curve slope but had no effect on the static stability.

5. Indenting a body for the purpose of increasing the skirt flare angle increased the static stability by a significant amount provided that the flared portion extends well into the airstream.

Langley Research Center,
National Aeronautics and Space Administration,
Langley Field, Va., August 11, 1958.

REFERENCES

1. Allen, H. Julian, and Eggers, A. J., Jr.: A Study of the Motion and Aerodynamic Heating of Missiles Entering the Earth's Atmosphere at High Supersonic Speeds. NACA TN 4047, 1957. (Supersedes NACA RM A53D28.)

2. Allen, H. Julian: Motion of a Ballistic Missile Angularly Misalined With the Flight Path Upon Entering the Atmosphere and Its Effect Upon Aerodynamic Heating, Aerodynamic Loads, and Miss Distance. NACA TN 4048, 1957. (Supersedes NACA RM A56F15.)

3. Braslow, Albert L.: Effect of Distributed Granular-Type Roughness on Boundary-Layer Transition at Supersonic Speeds With and Without Surface Cooling. NACA RM L58A17, 1958.

4. Burrows, Dale L., and Palmer, William E.: A Transonic Wind-Tunnel Investigation of the Force and Moment Characteristics of a Plane and a Cambered 3-Percent-Thick Delta Wing of Aspect Ratio 3 on a Slender Body. NACA RM L54H25, 1954.

5. Polhamus, Edward C.: Effect of Flow Incidence and Reynolds Number on Low-Speed Aerodynamic Characteristics of Several Noncircular Cylinders With Applications to Directional Stability and Spinning. NACA TN 4176, 1958.

TABLE I.– PRESENTATION OF DATA

Model	Figures containing data
 1	5, 6, 7, 24, 30(c)
 3	5, 7, 24
 4	5, 6, 7, 24, 30(c)
 5	6, 7, 24
 7	8, 10, 11, 12, 13, 14, 18, 19, 20, 21, 25, 26, 27, 29, 30(a), 30(b)
 7a	8, 25, 30(a)
 7b	8, 25, 30(a), 31
 7-15	13, 14, 26, 30(a)
 7-30	13, 14, 26, 30(a)
 8	10, 11, 12, 27, 30(b)
 9	9, 10, 11, 12, 27, 30(b)
 9b	9

Model	Figures containing data
 10	11, 12, 27, 30(b)
 11	23
 12	15, 16, 17, 28, 30(c)
 13	15, 16, 17, 28, 30(c)
 14	15, 16, 17, 28, 30(a)
 17	22
 18	18, 19, 21, 29, 30(b)
 19	18, 19, 21, 29, 30(b)
 20	20, 21, 29
 21	20, 21, 29
 22	20, 21, 29

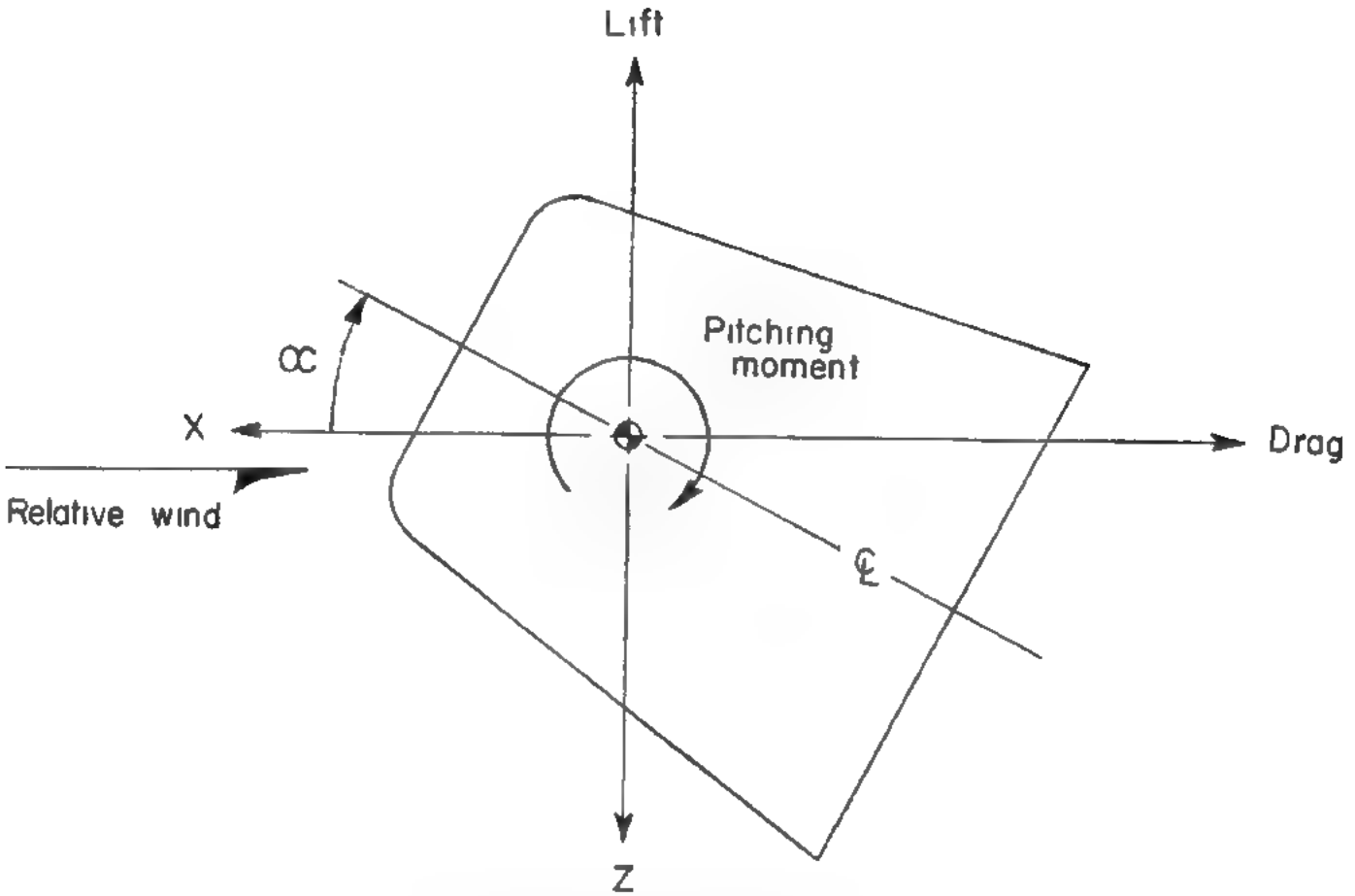

Figure 1.- System of stability axes. Arrows indicate positive directions of forces, moments, and angular displacements.

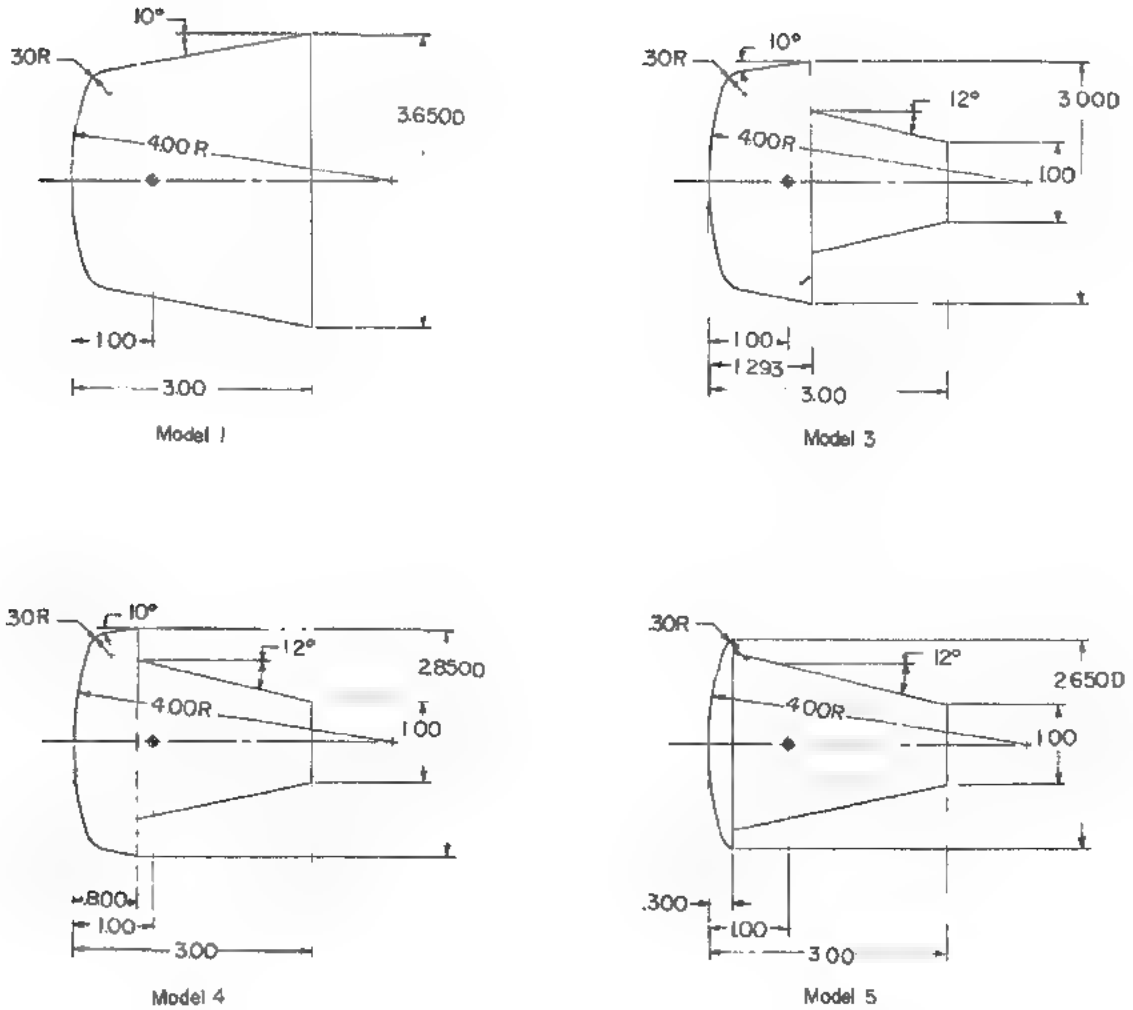

(a) Skirt-length family.

Figure 2.- Drawings of model tested. All dimensions are in inches.

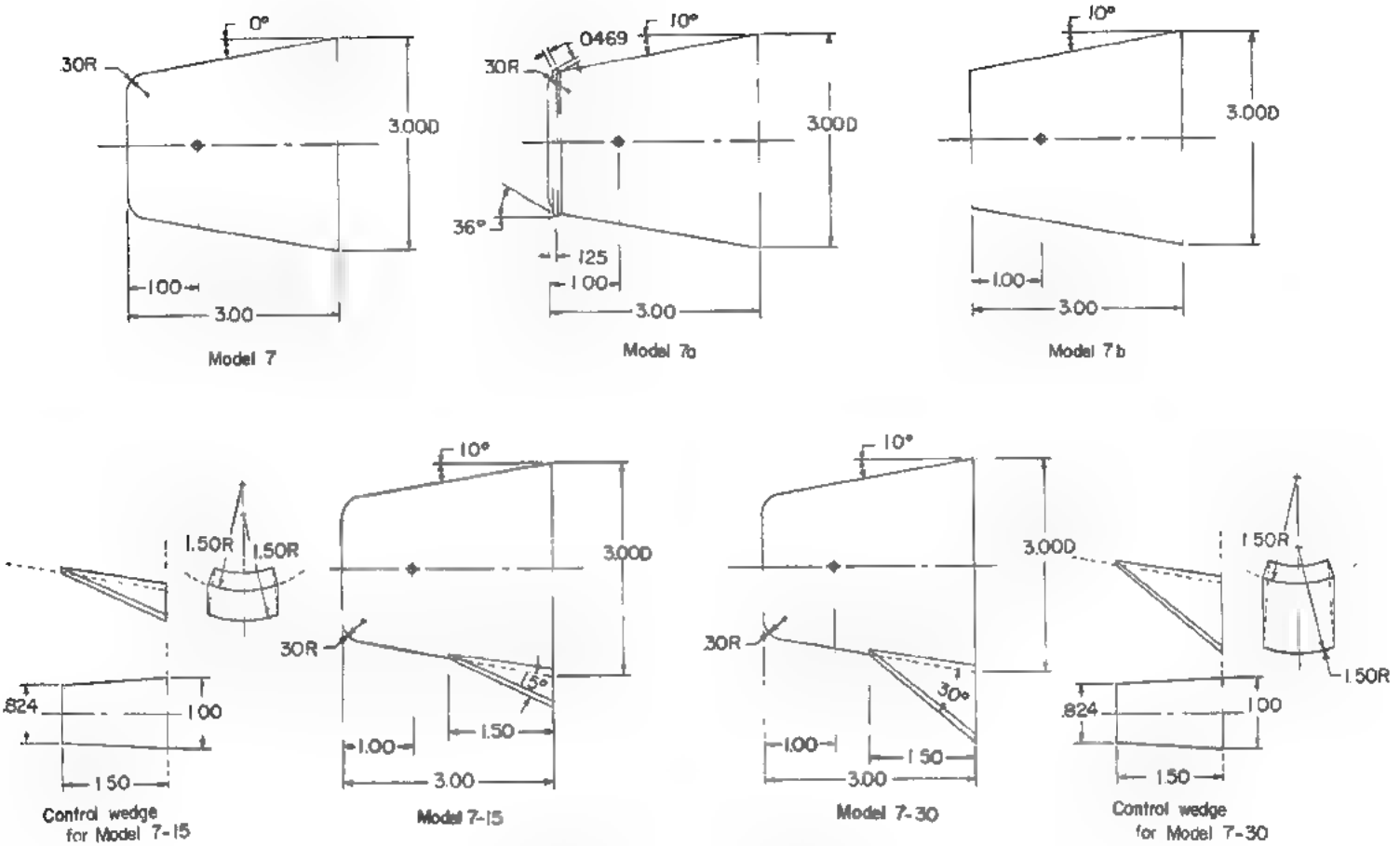

(b) Shoulder-radius and deflected-control families.

Figure 2.- Continued.

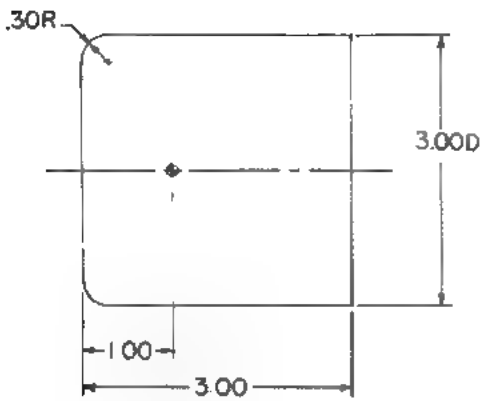

Model 8

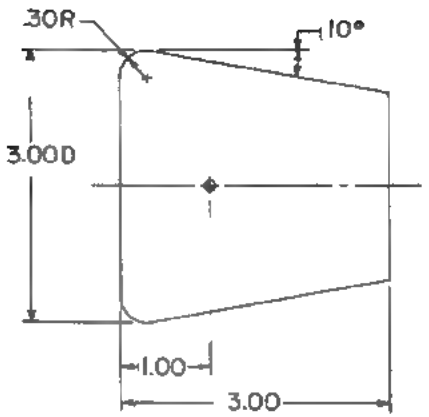

Model 9

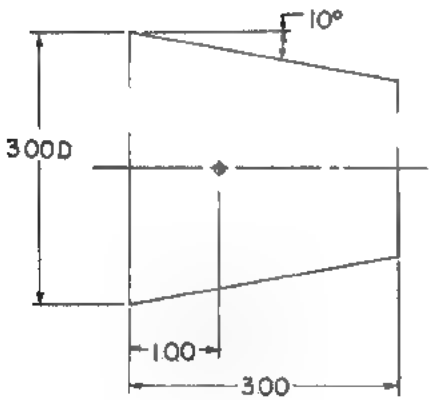

Model 9b

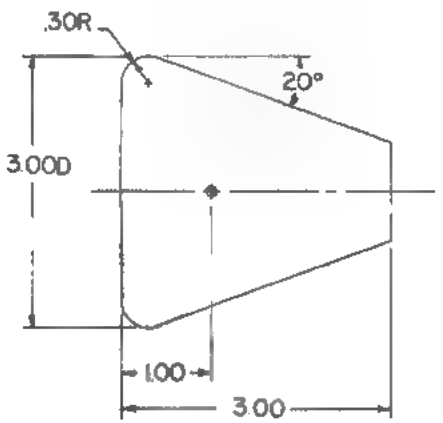

Model 10

(c) Body-slope family.

Figure 2.- Continued.

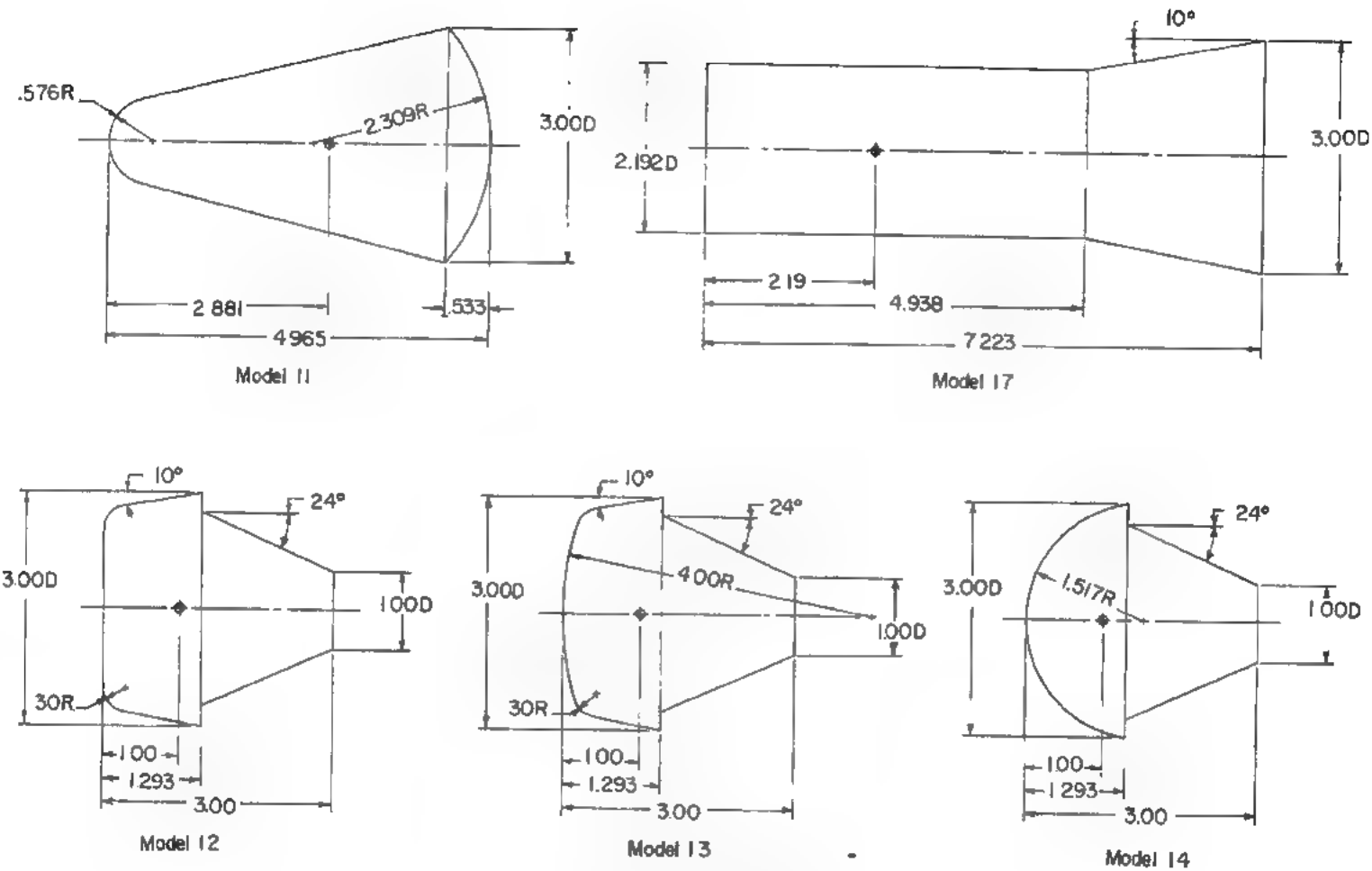

(d) Nose-radius family and miscellaneous models.

Figure 2.- Continued.

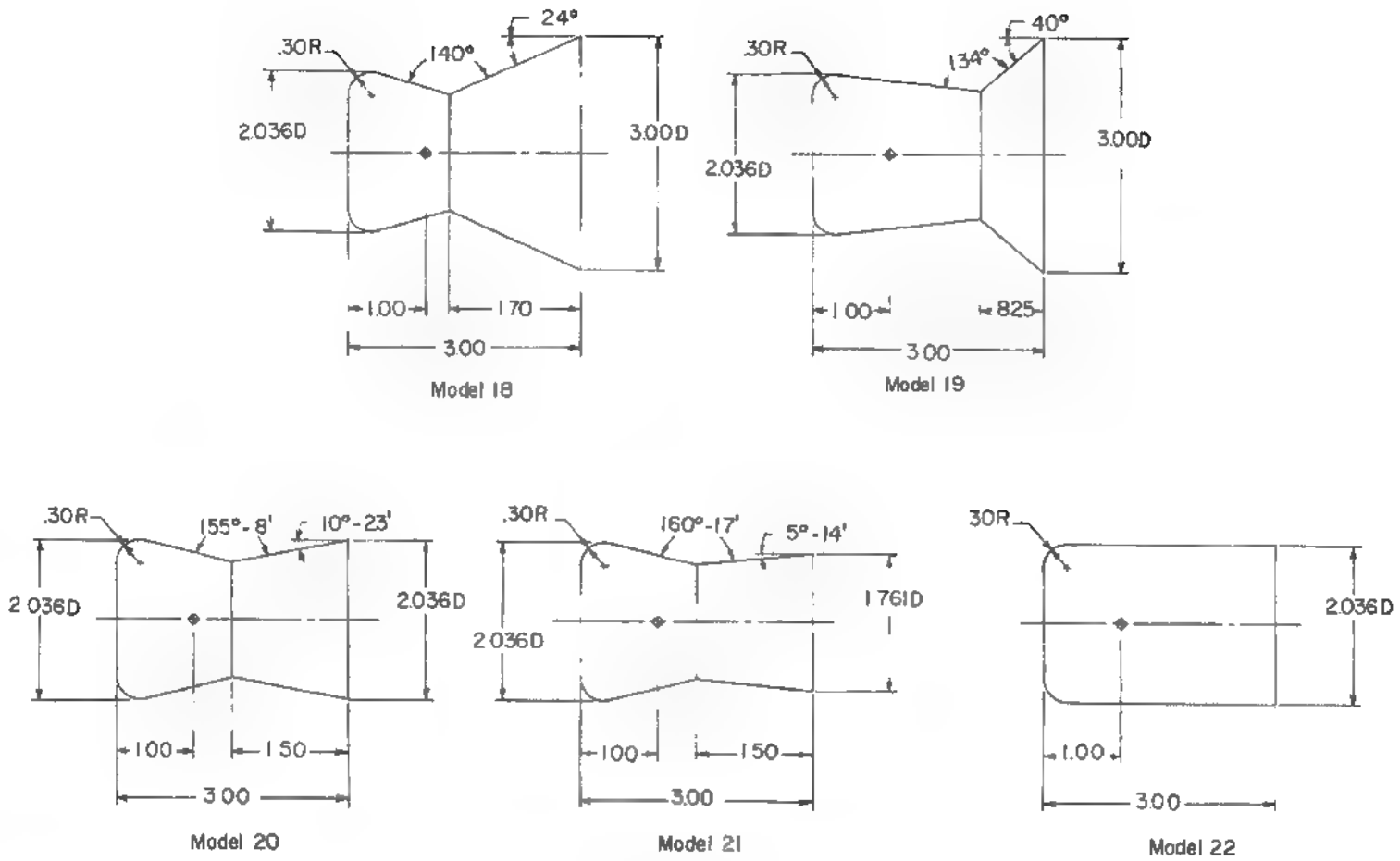

(e) Indented-body family.

Figure 2.- Concluded.

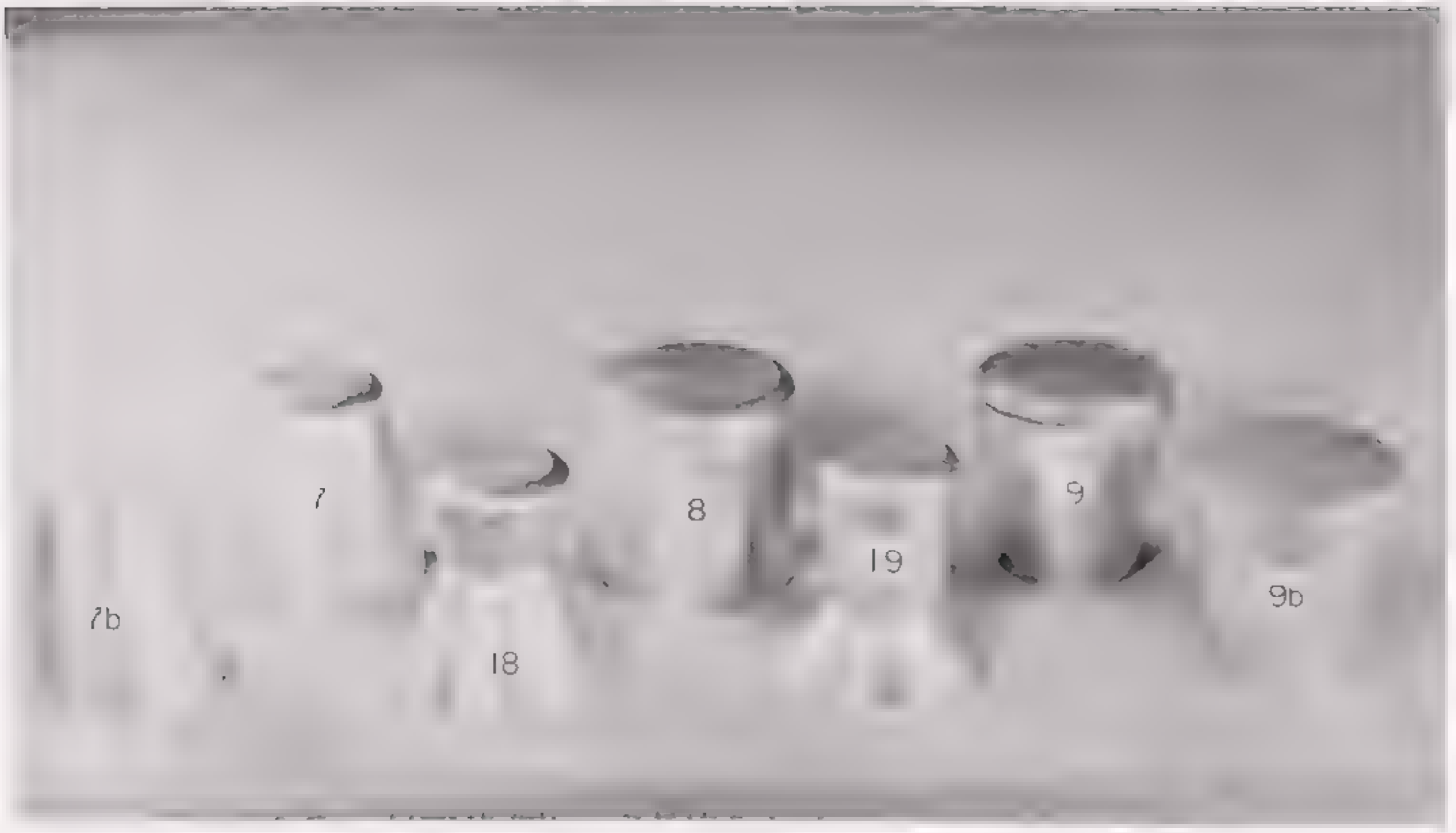
7
8
9
7b
18
19
9b

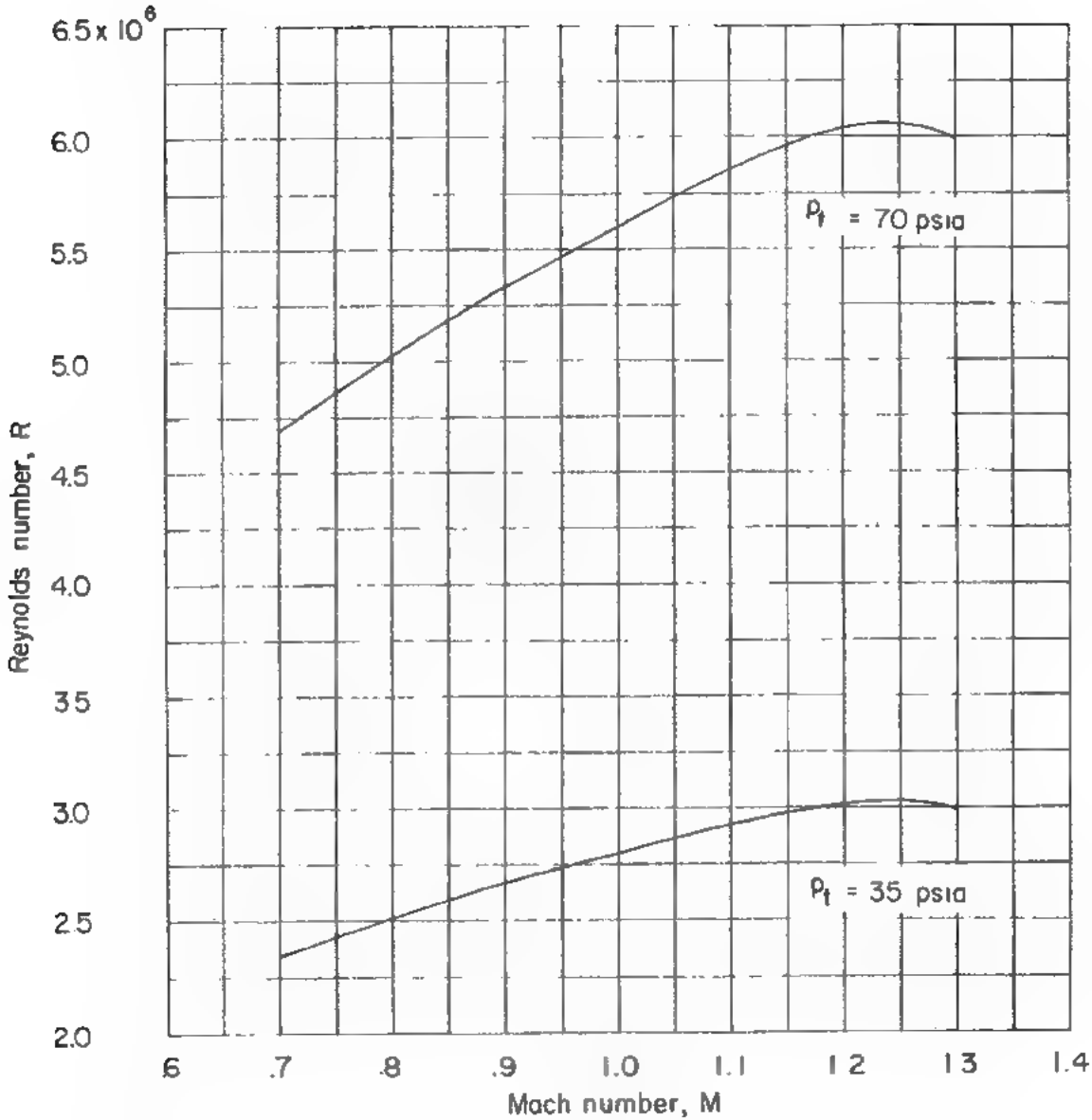

Figure 4.- Variation of Reynolds number (based on body length of 3 inches) with Mach number for two test stagnation pressures.

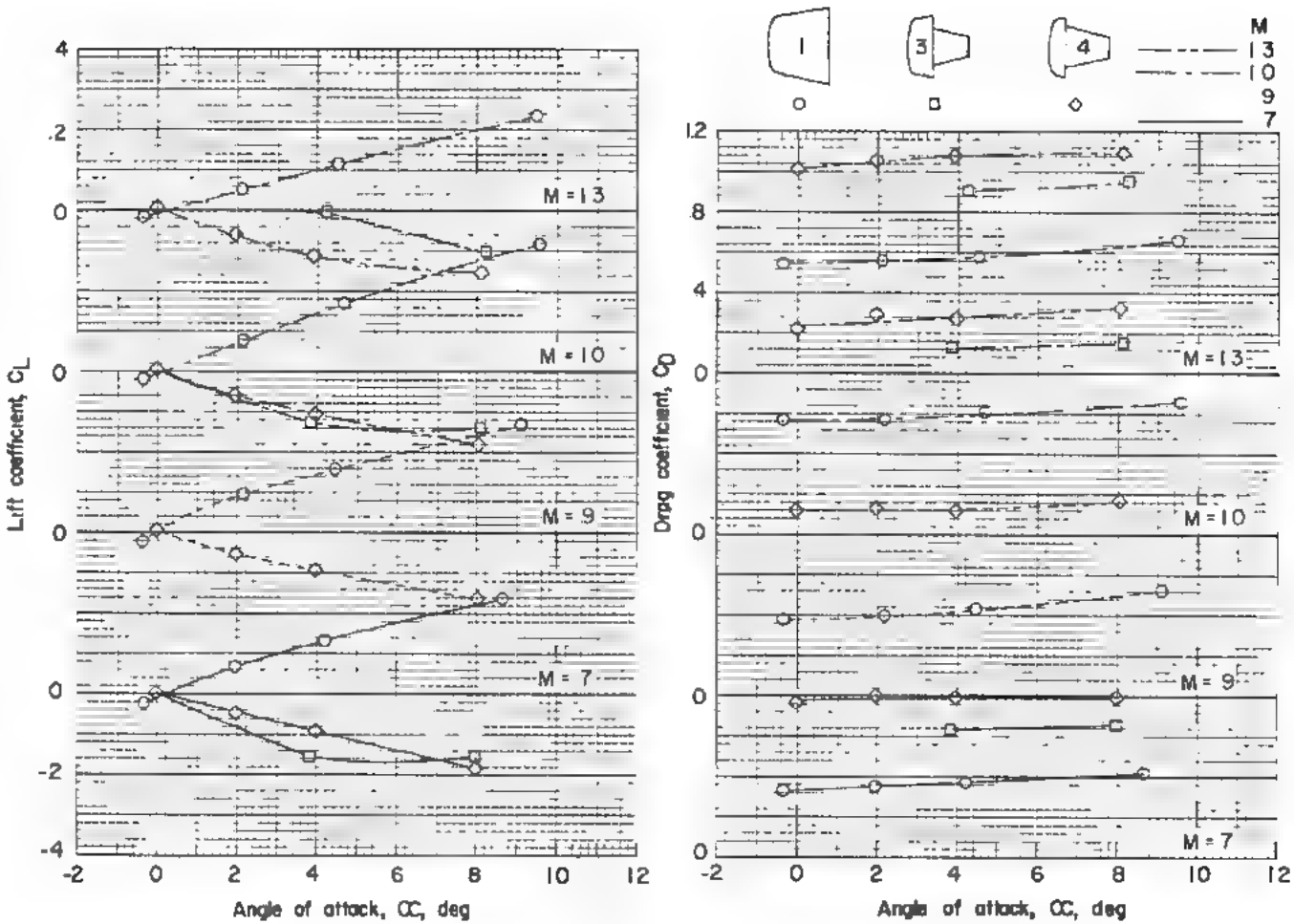

(a) Lift coefficient.

(b) Drag coefficient.

Figure 5.- Effect of a reduction in afterbody length on the lift, drag, and pitching-moment coefficients for a family of blunt shapes; p_t = 70 psia.

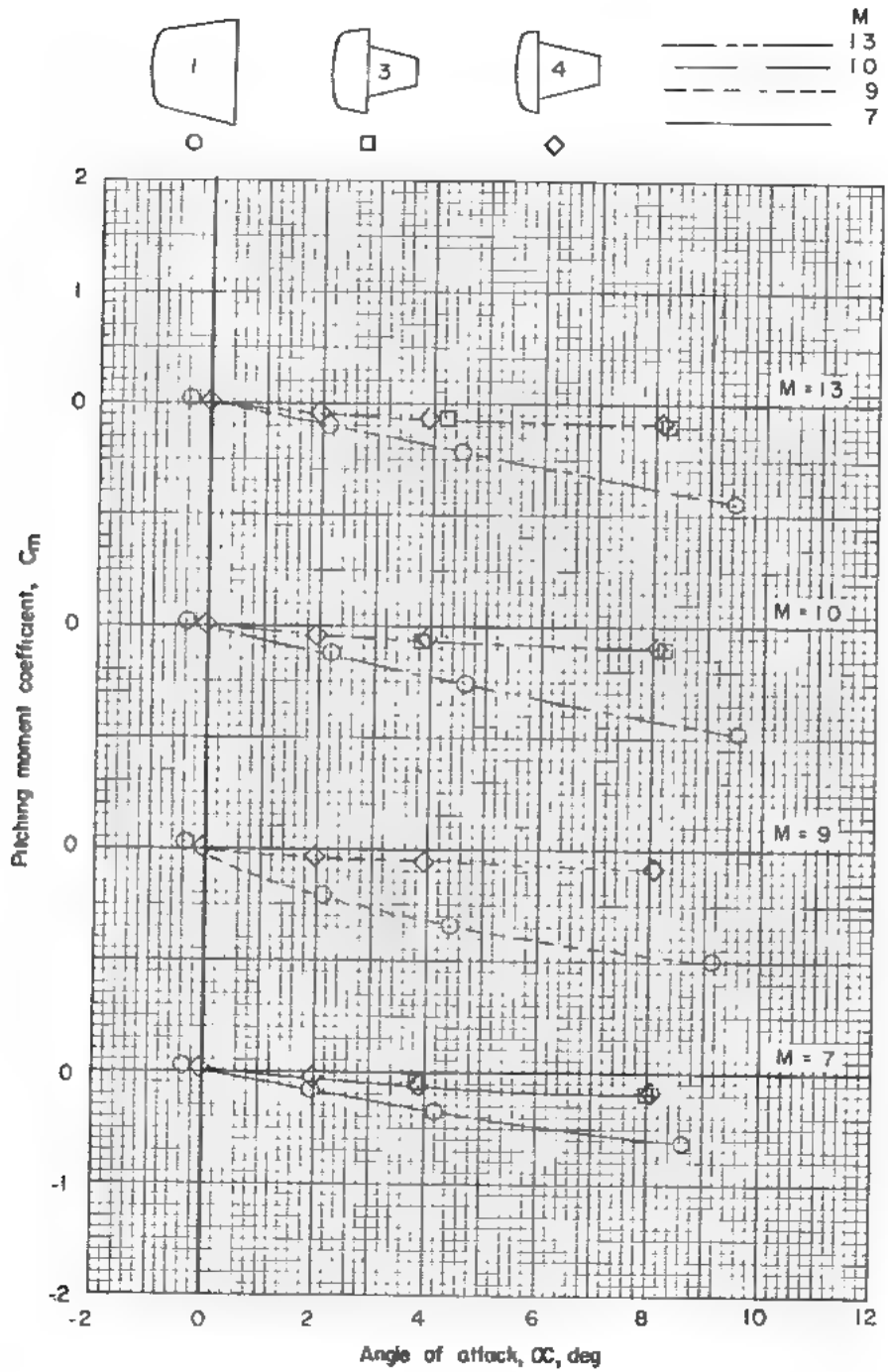

(c) Pitching-moment coefficient.

Figure 5.- Concluded.

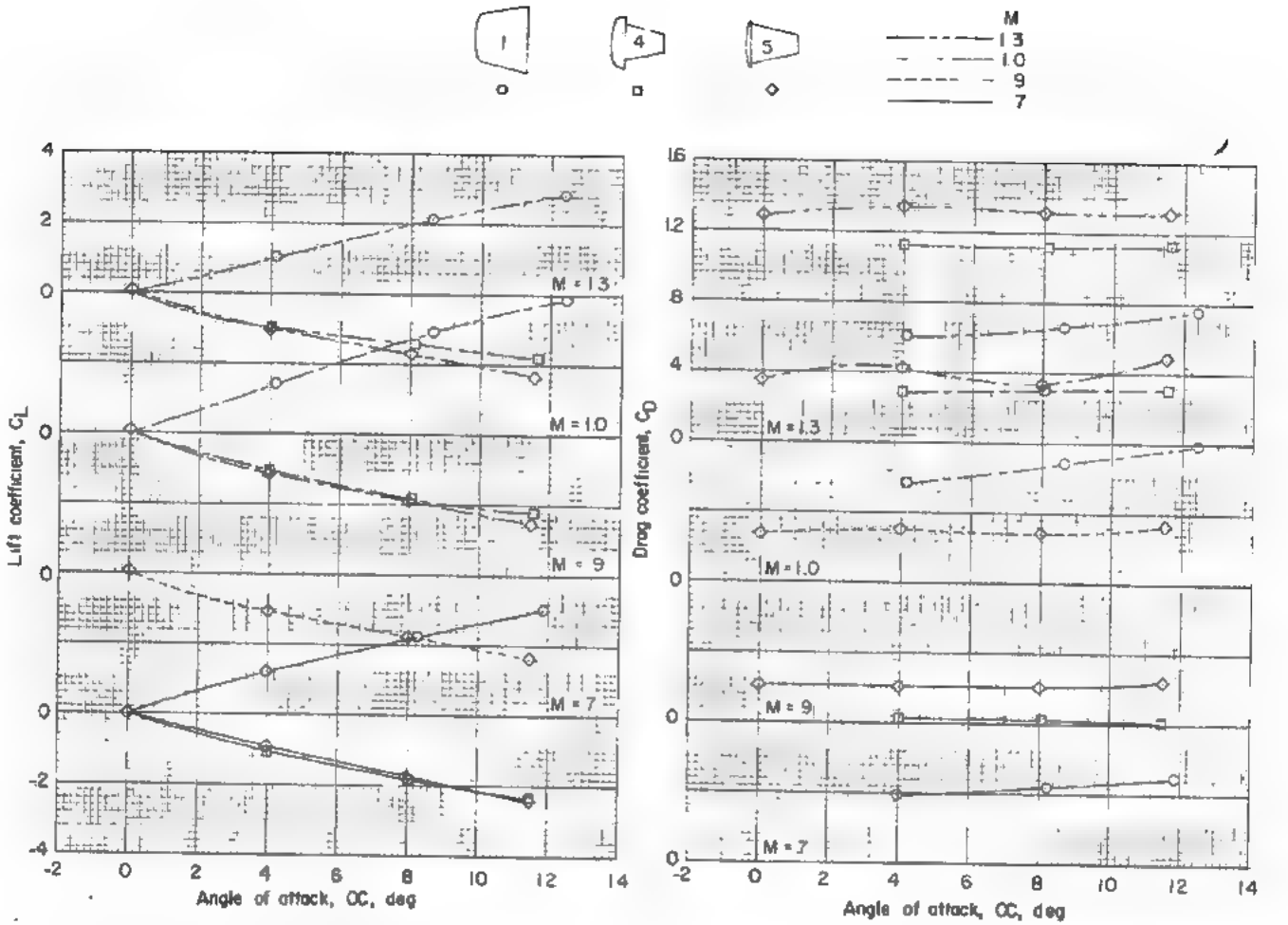

(a) Lift coefficient.

(b) Drag coefficient.

Figure 6.- Effect of a reduction in skirt length on the lift, drag, and pitching-moment coefficients for a family of blunt bodies; p_t = 35 psia.

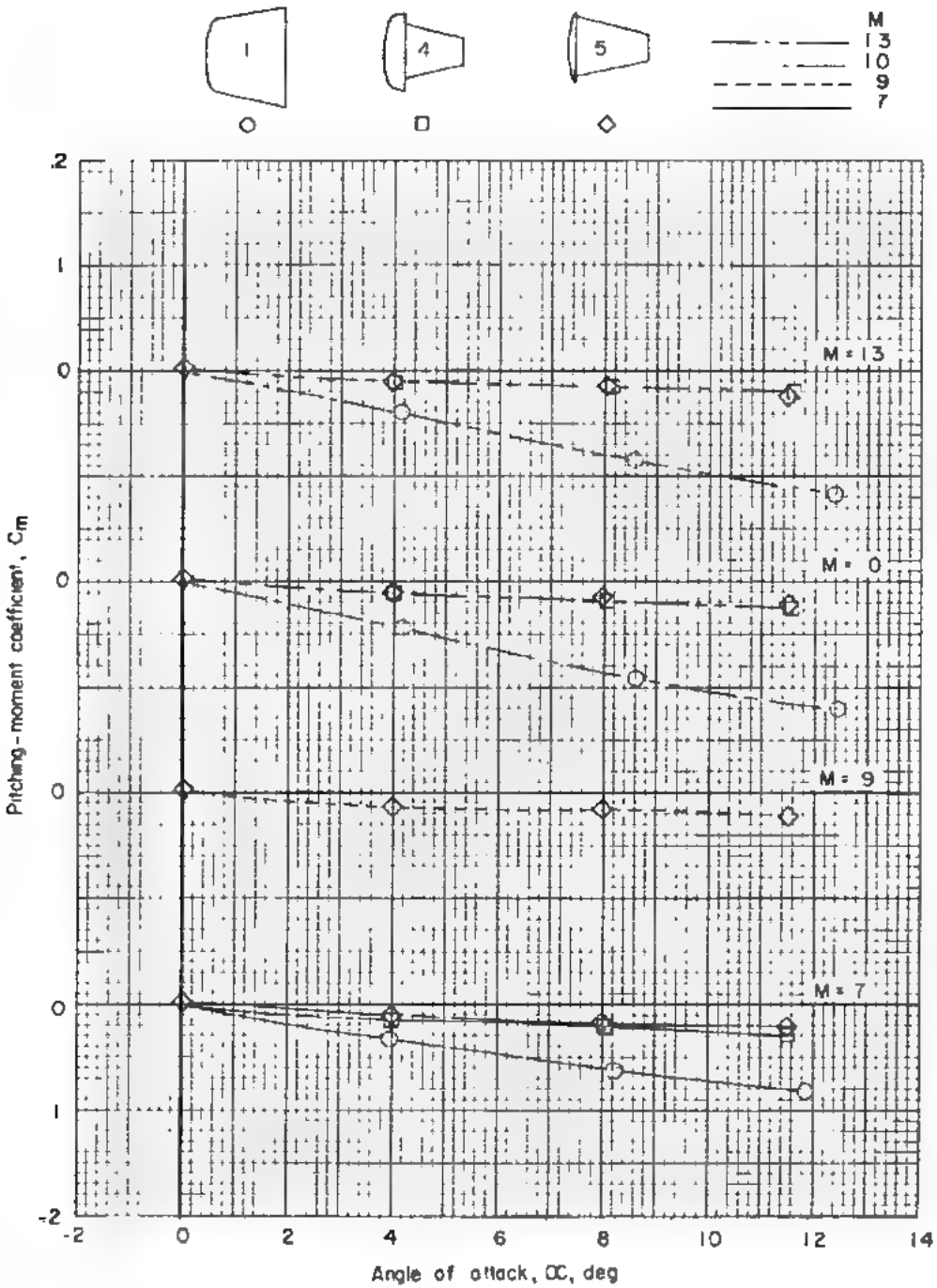

(c) Pitching-moment coefficients.

Figure 6.- Concluded.

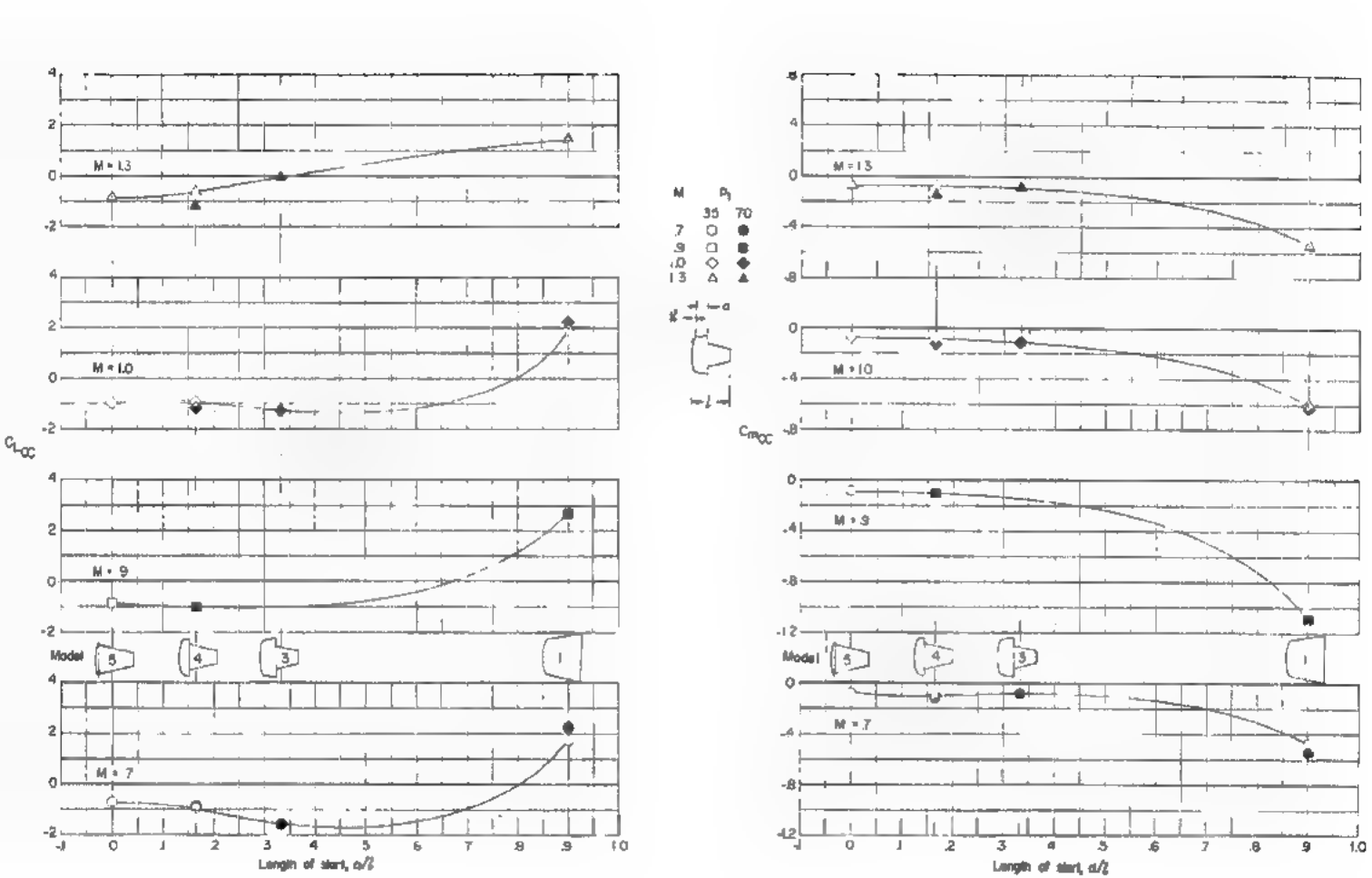

Figure 7.- Effect of the length of the skirt on the longitudinal stability derivatives for a family of blunt bodies.

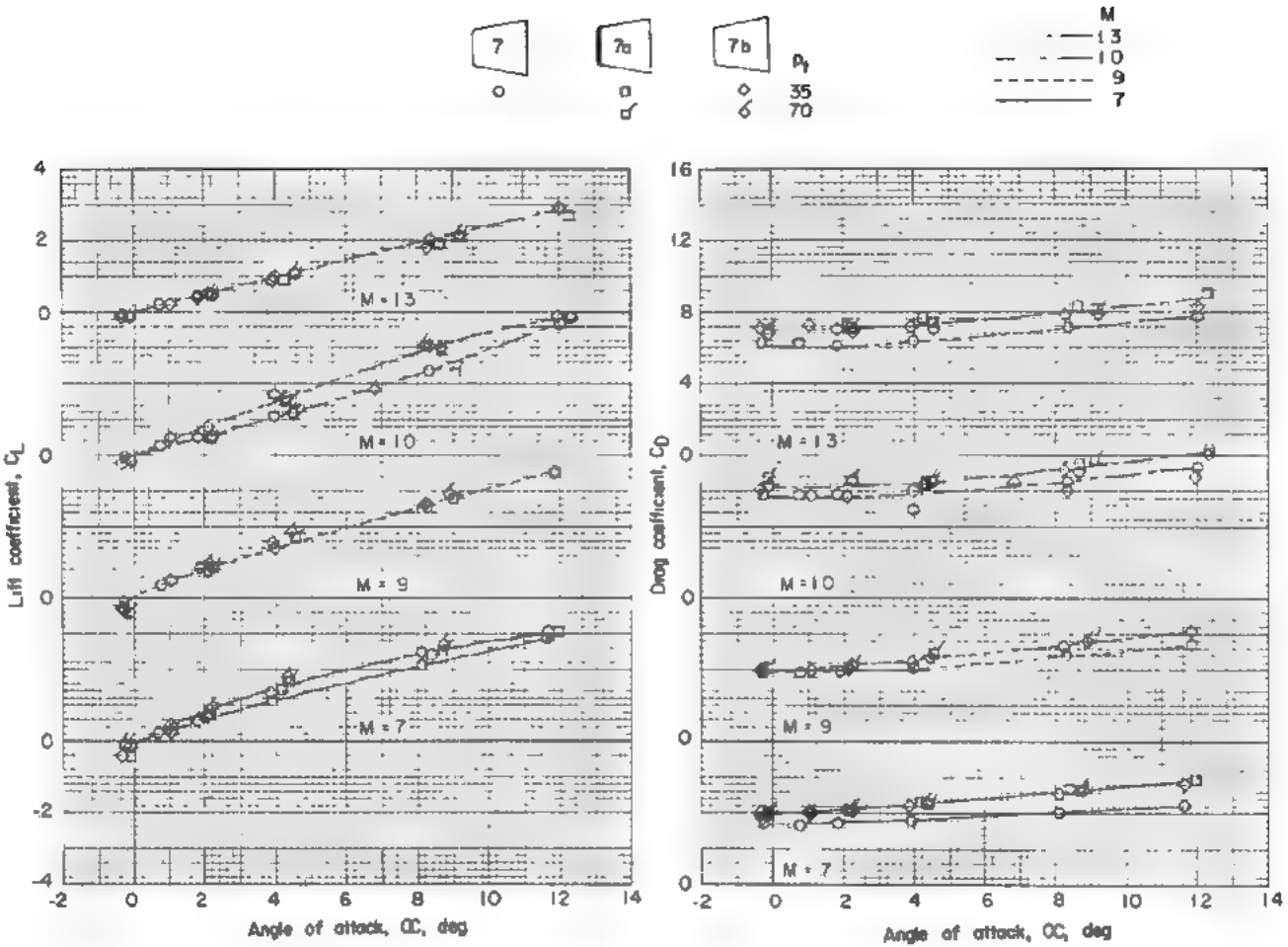

(a) Lift coefficient.

(b) Drag coefficient.

Figure 8.- Effect of a shoulder radius and a nose ring on the lift, drag, and pitching-moment coefficients for a family of blunt bodies.

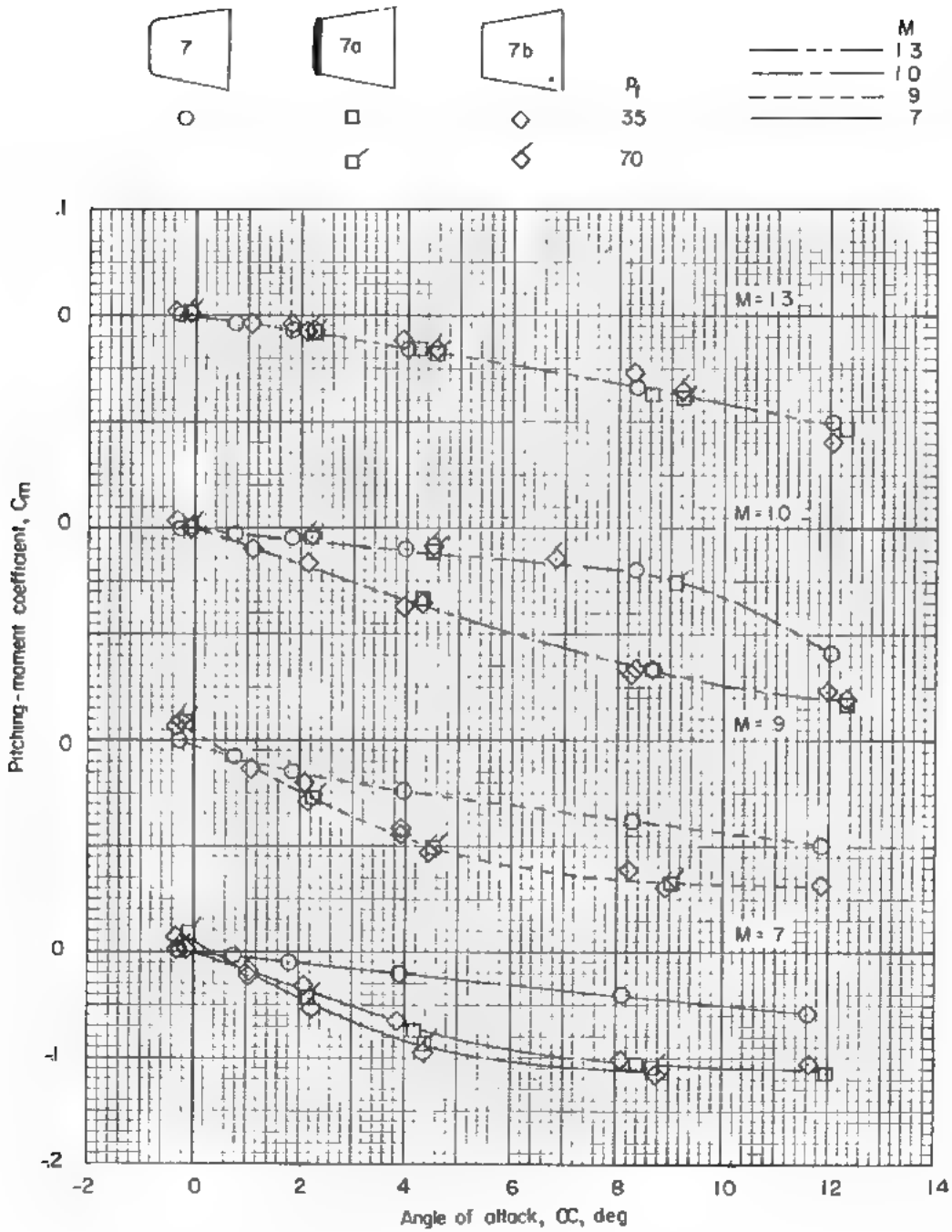

(c) Pitching-moment coefficient.

Figure 8.- Concluded.

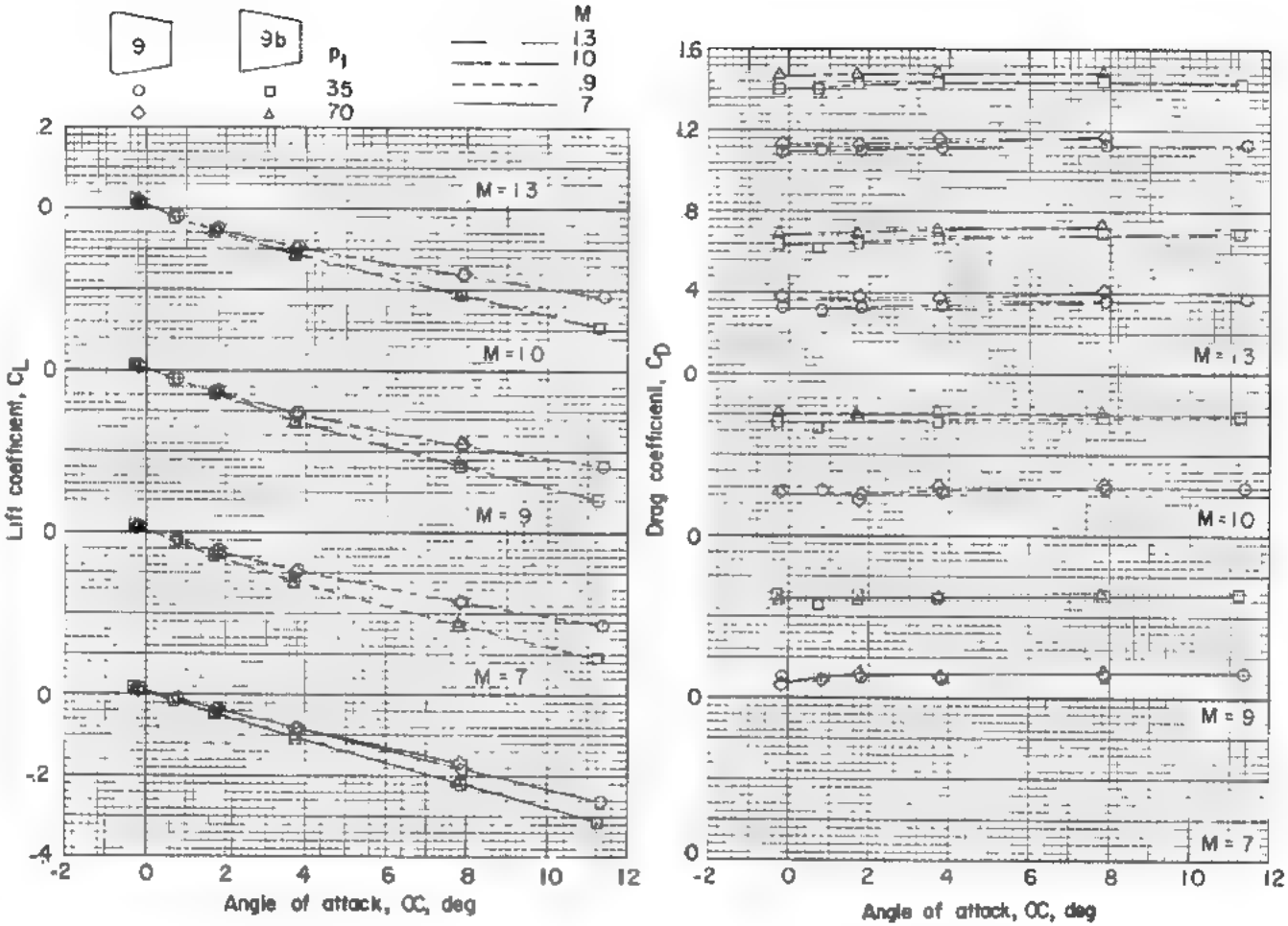

(a) Lift coefficient.

(b) Drag coefficient.

Figure 9.- Effect of shoulder radius on the lift, drag, and pitching-moment coefficients for a blunt body.

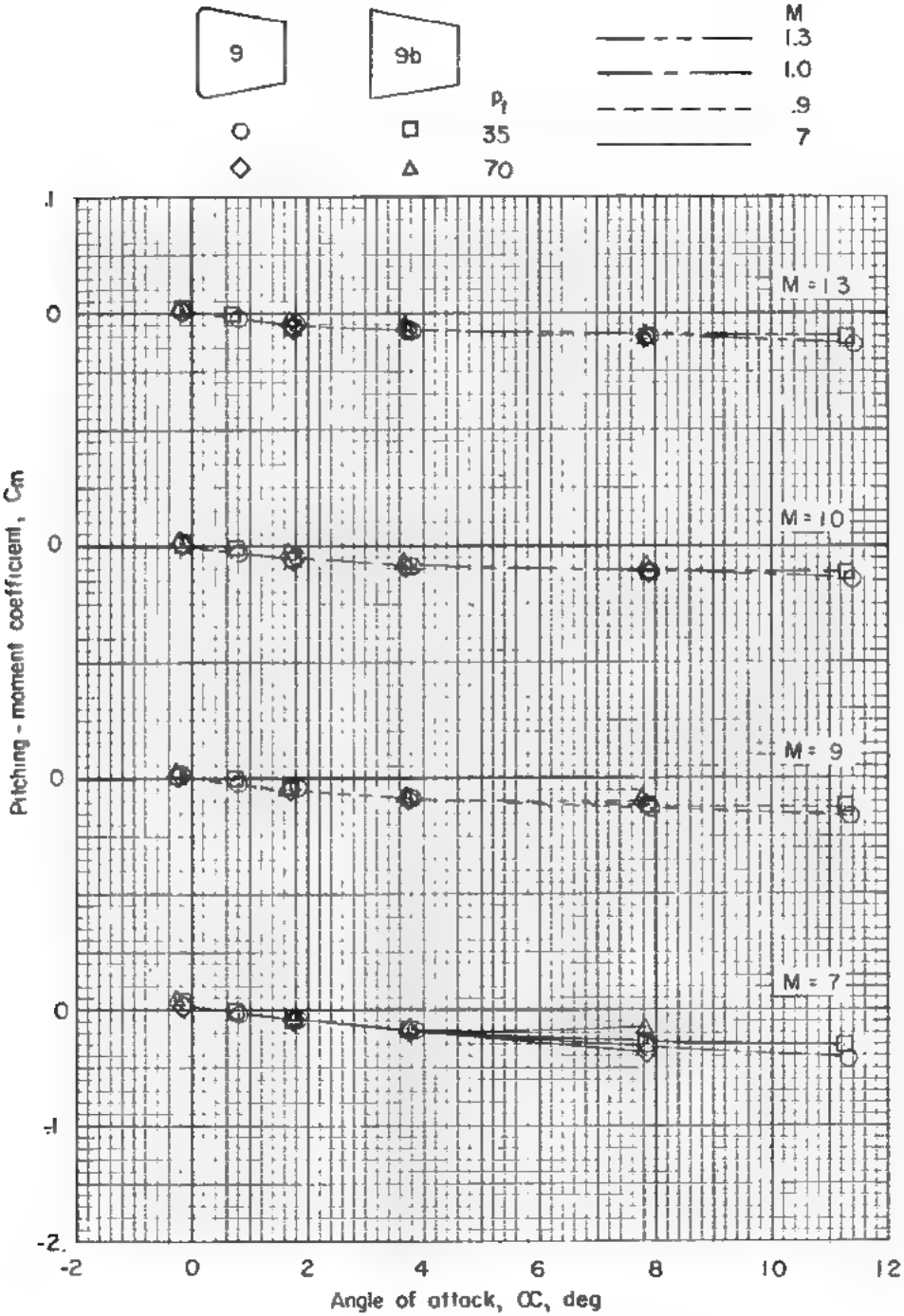

(c) Pitching-moment coefficient.

Figure 9.- Concluded.

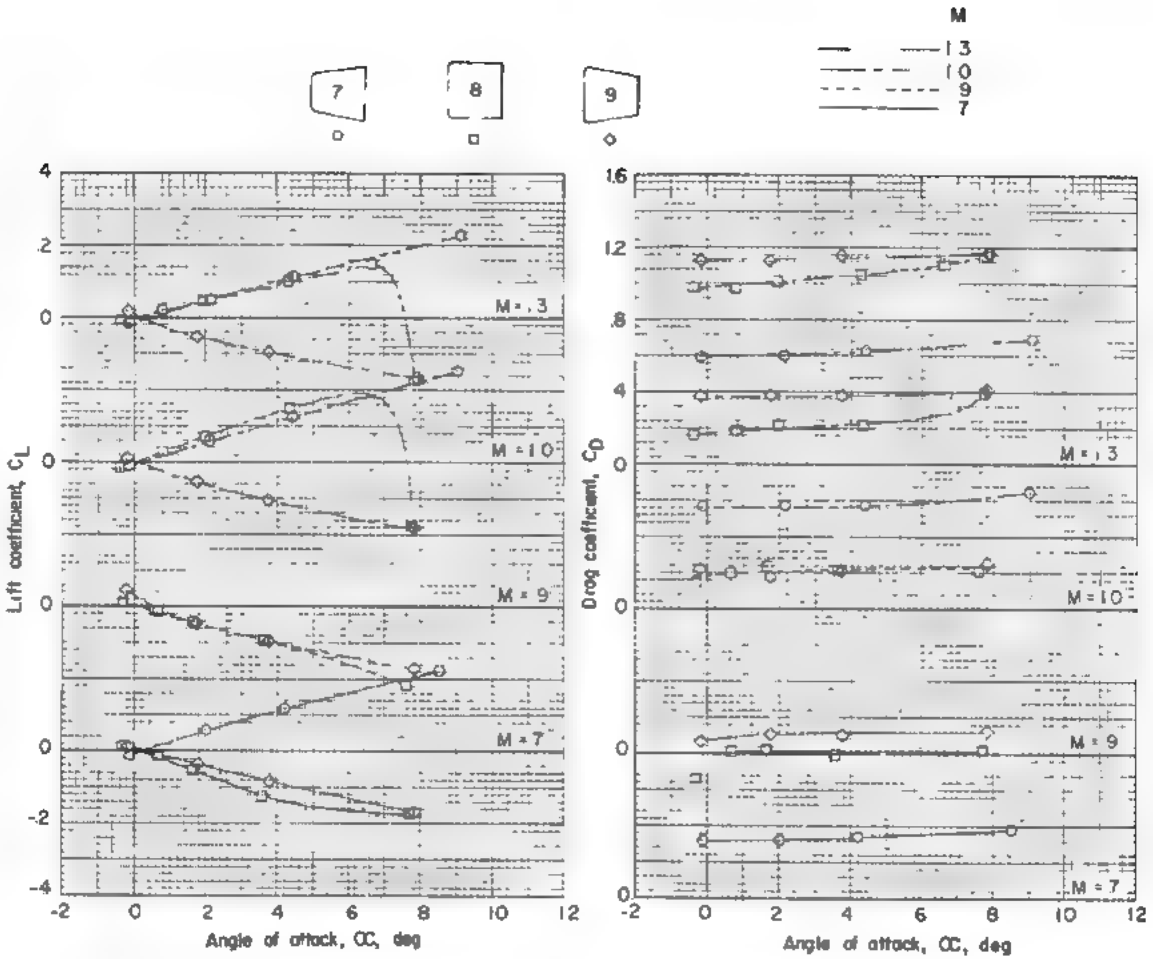

(a) Lift coefficient.

(b) Drag coefficient.

Figure 10.- Effect of slope of the body on the lift, drag, and pitching-moment coefficients for a family of blunt bodies; p_t = 70 psia.

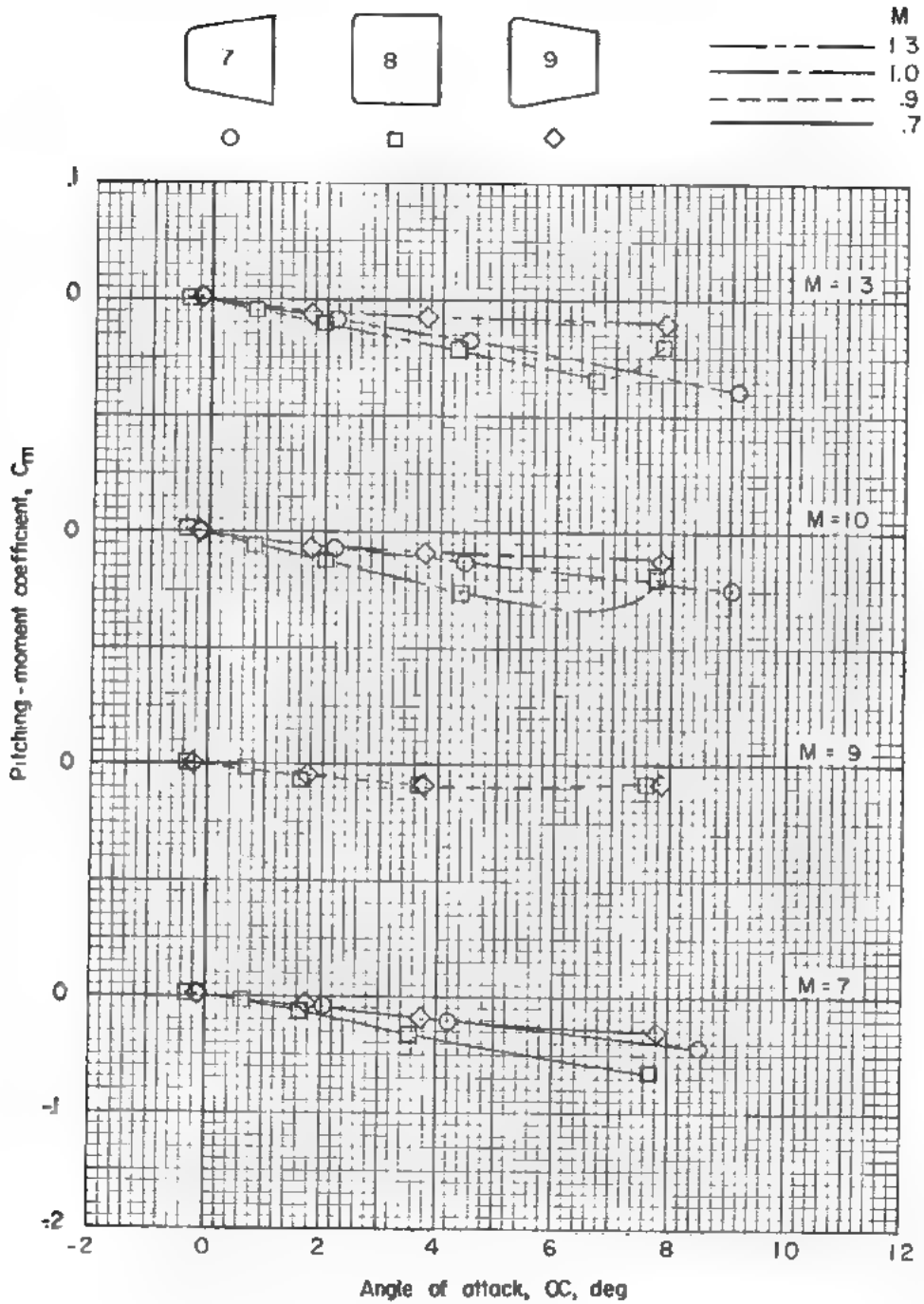

(c) Pitching-moment coefficient.

Figure 10.- Concluded.

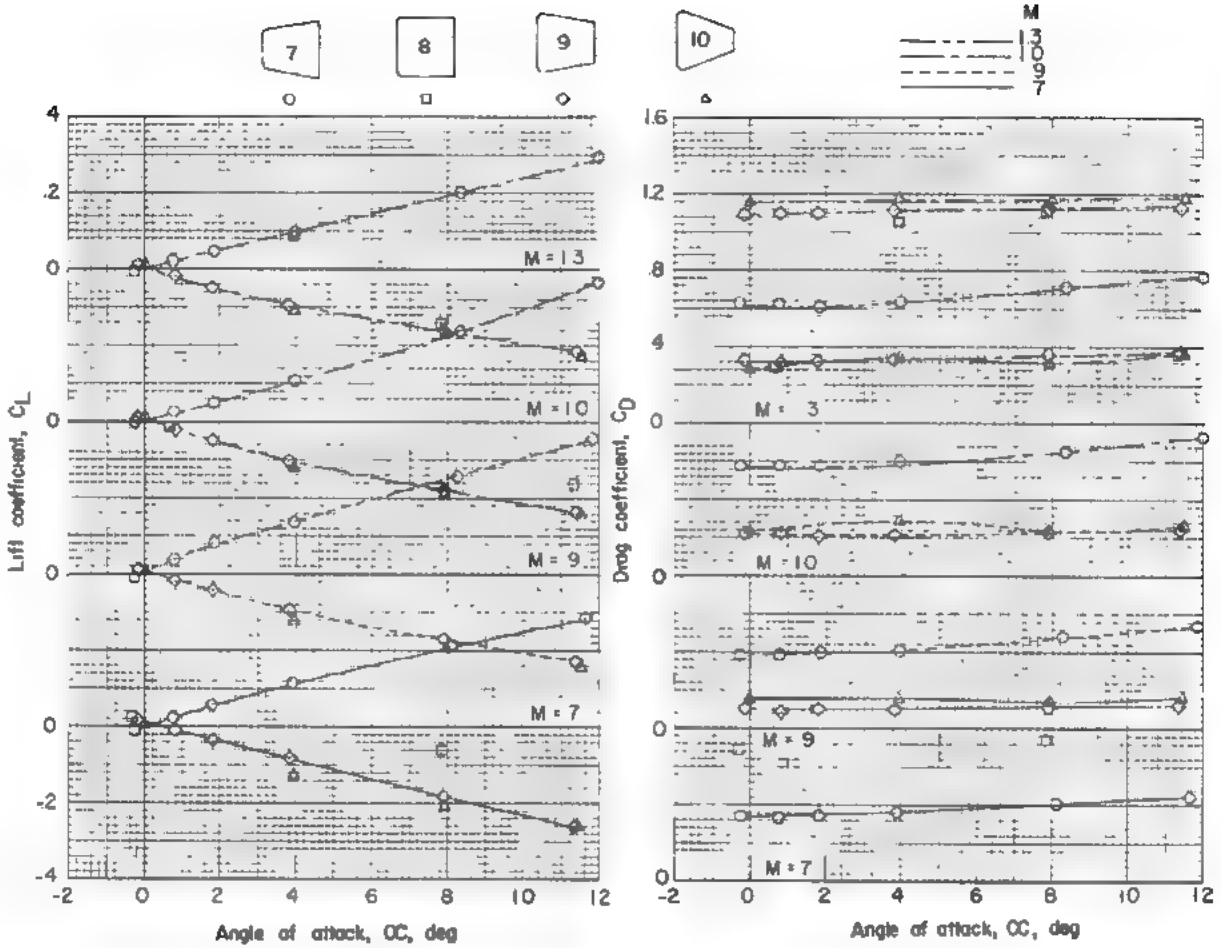

(a) Lift coefficient.

(b) Drag coefficient.

Figure 11.- Effect of slope of the body on the lift, drag, and pitching-moment coefficients for a family of blunt bodies; p_t = 35 psia.

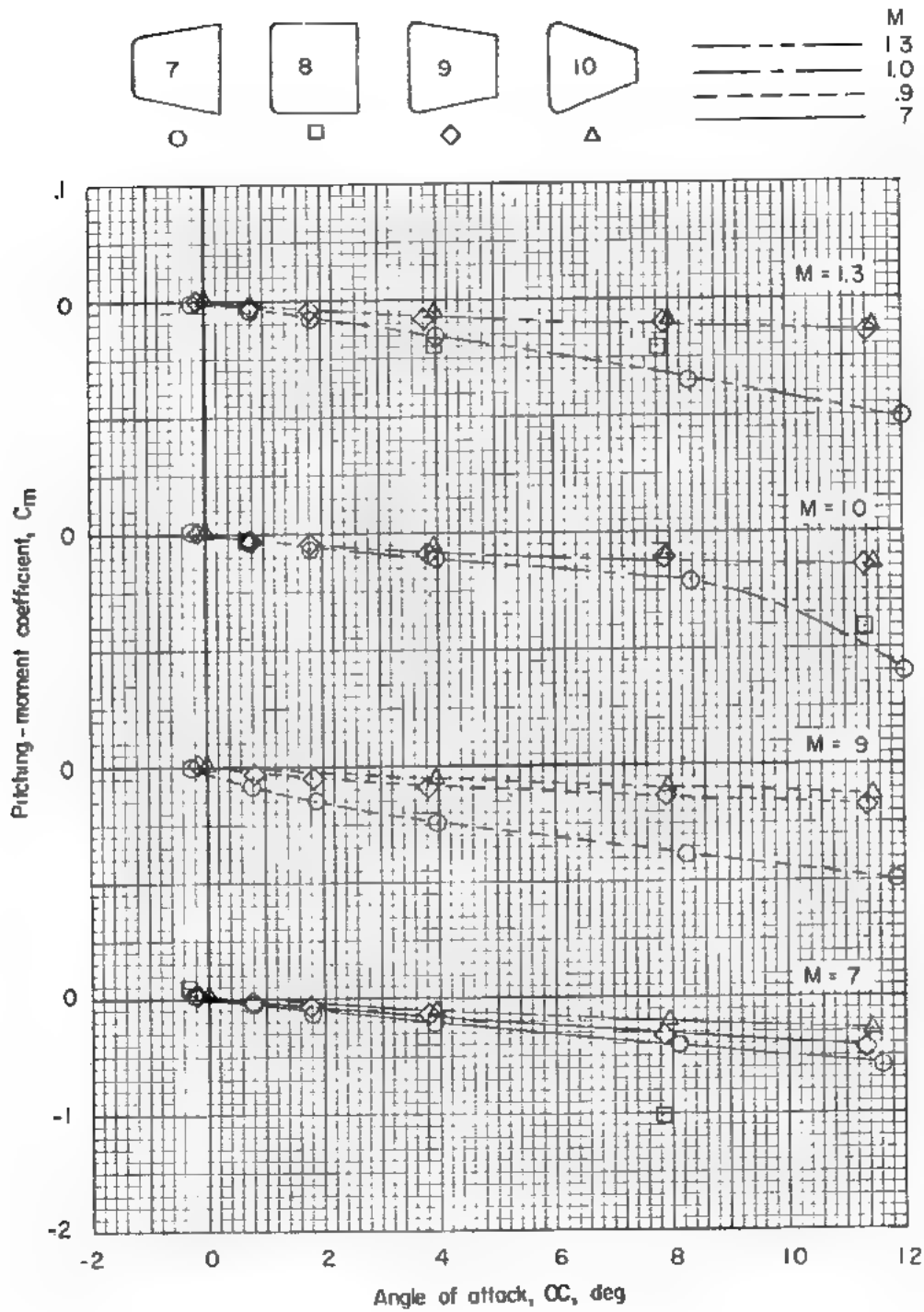

(c) Pitching-moment coefficient.

Figure 11.- Concluded.

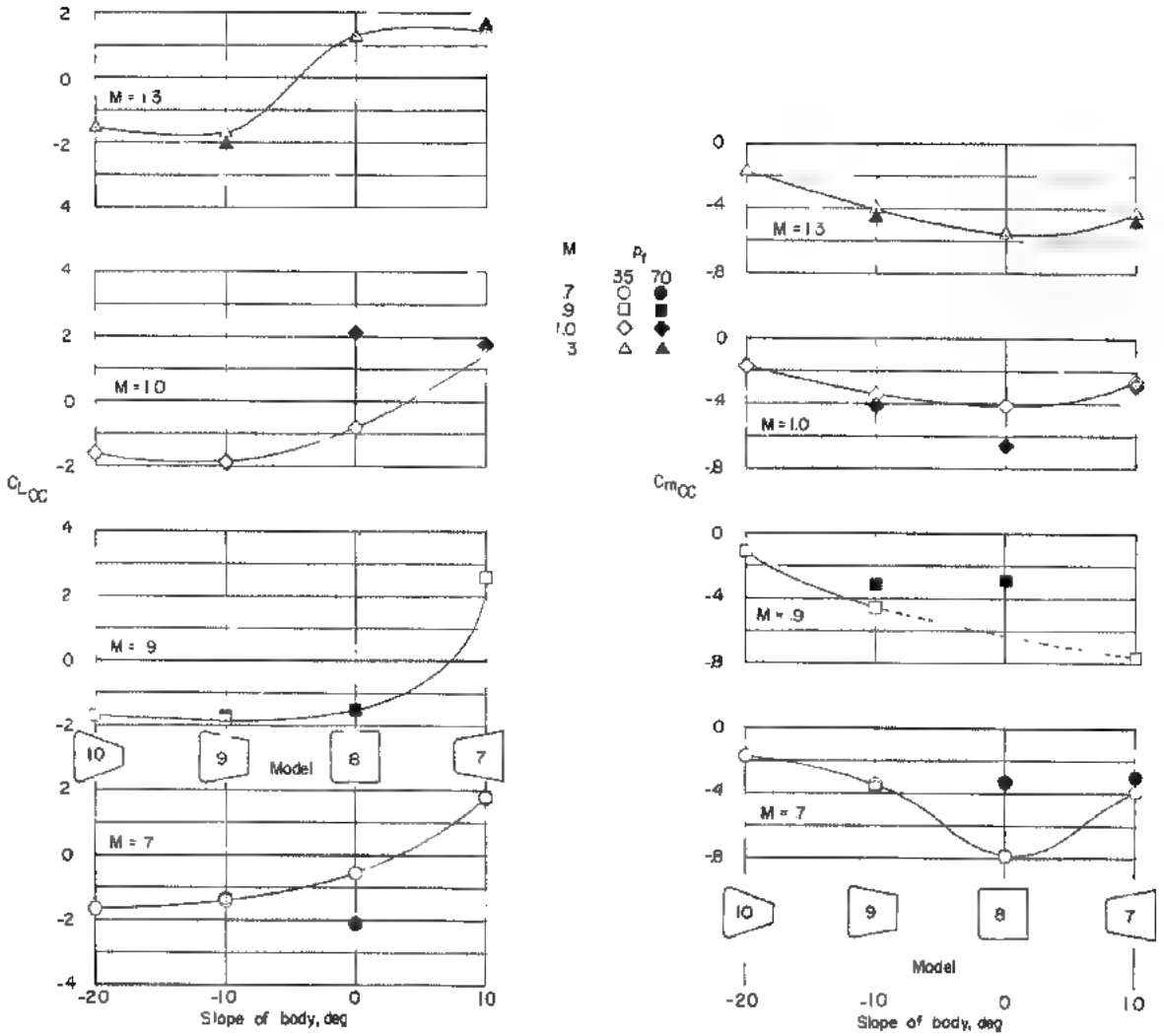

Figure 12.- Effect of the slope of the body on the longitudinal stability derivatives for a family of blunt bodies.

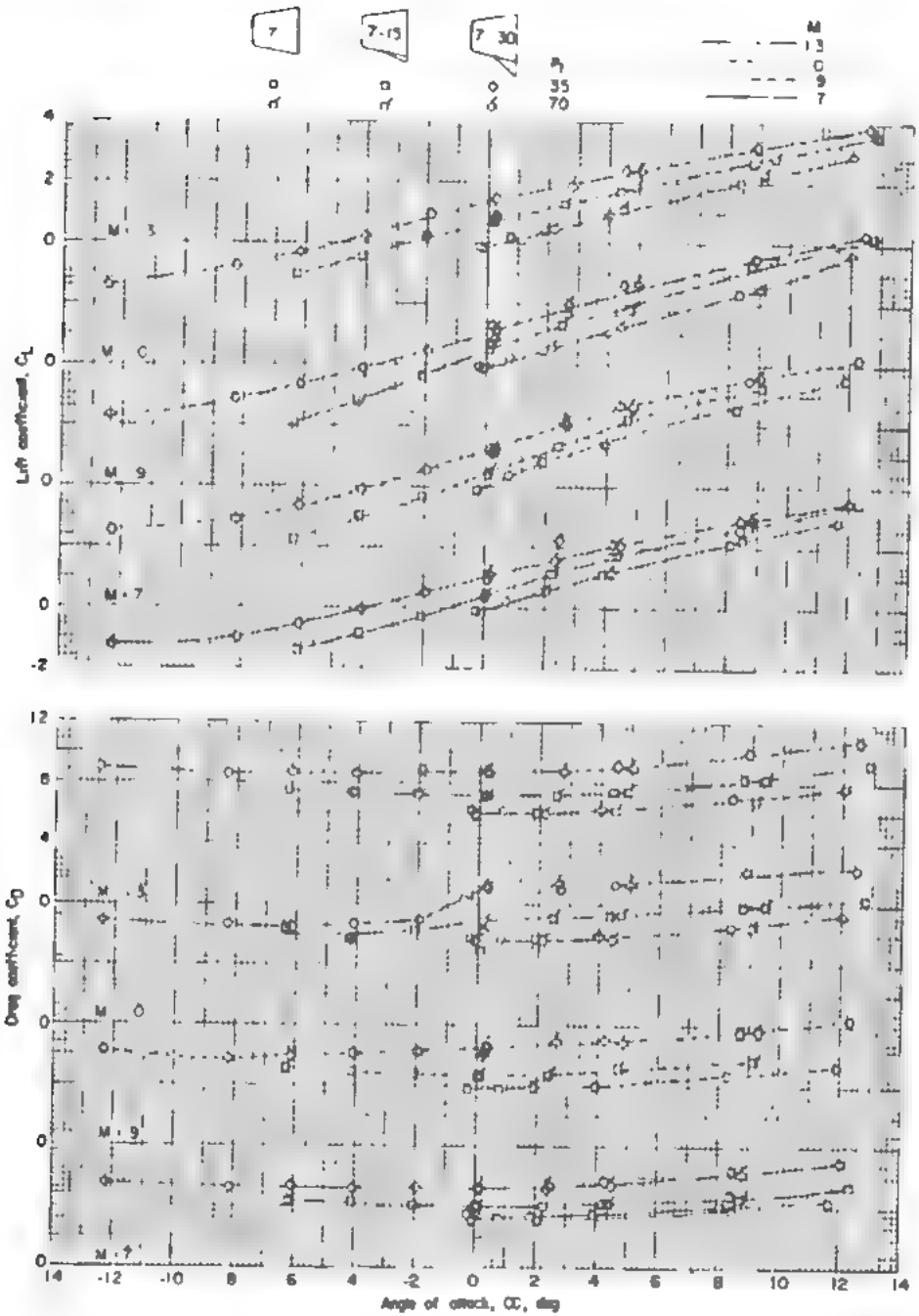

(a) Lift and drag coefficients.

Figure 13.- Effect of a control-wedge deflection on the lift, drag, and pitching-moment coefficients of a blunt body.

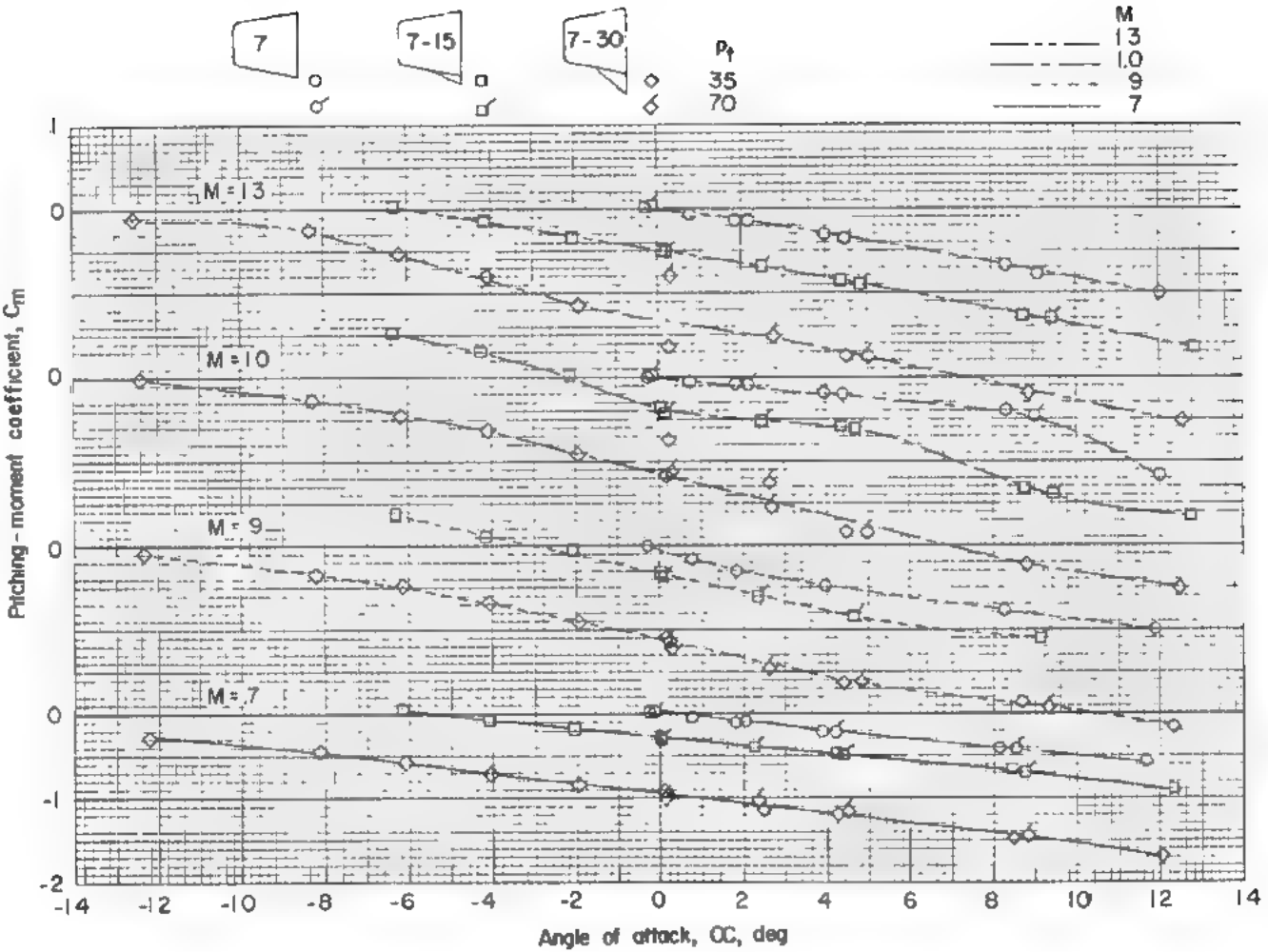

(b) Pitching-moment coefficient.

Figure 13.- Concluded.

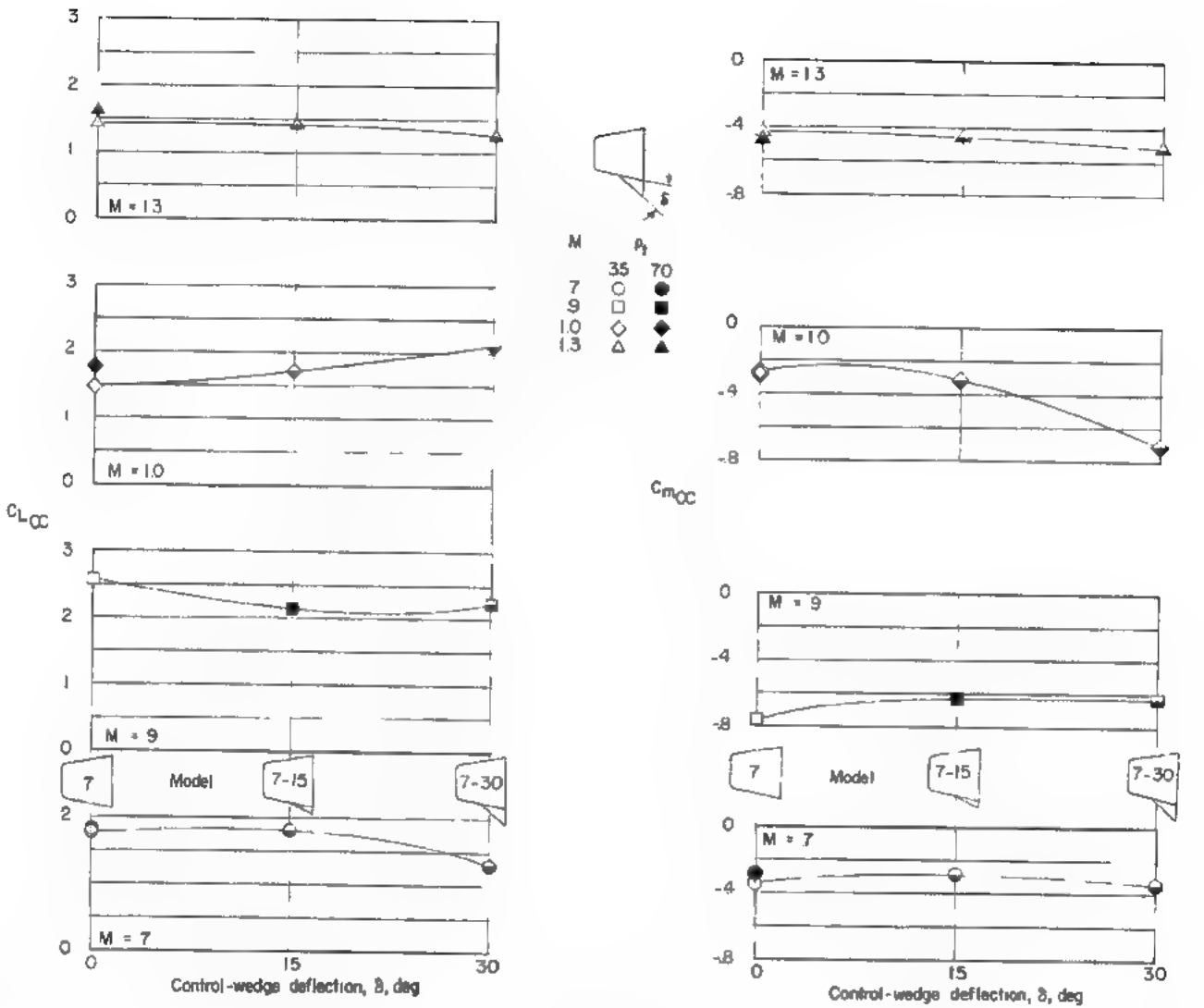

Figure 14.- Effect of control-wedge deflection on the longitudinal stability derivatives for a blunt body.

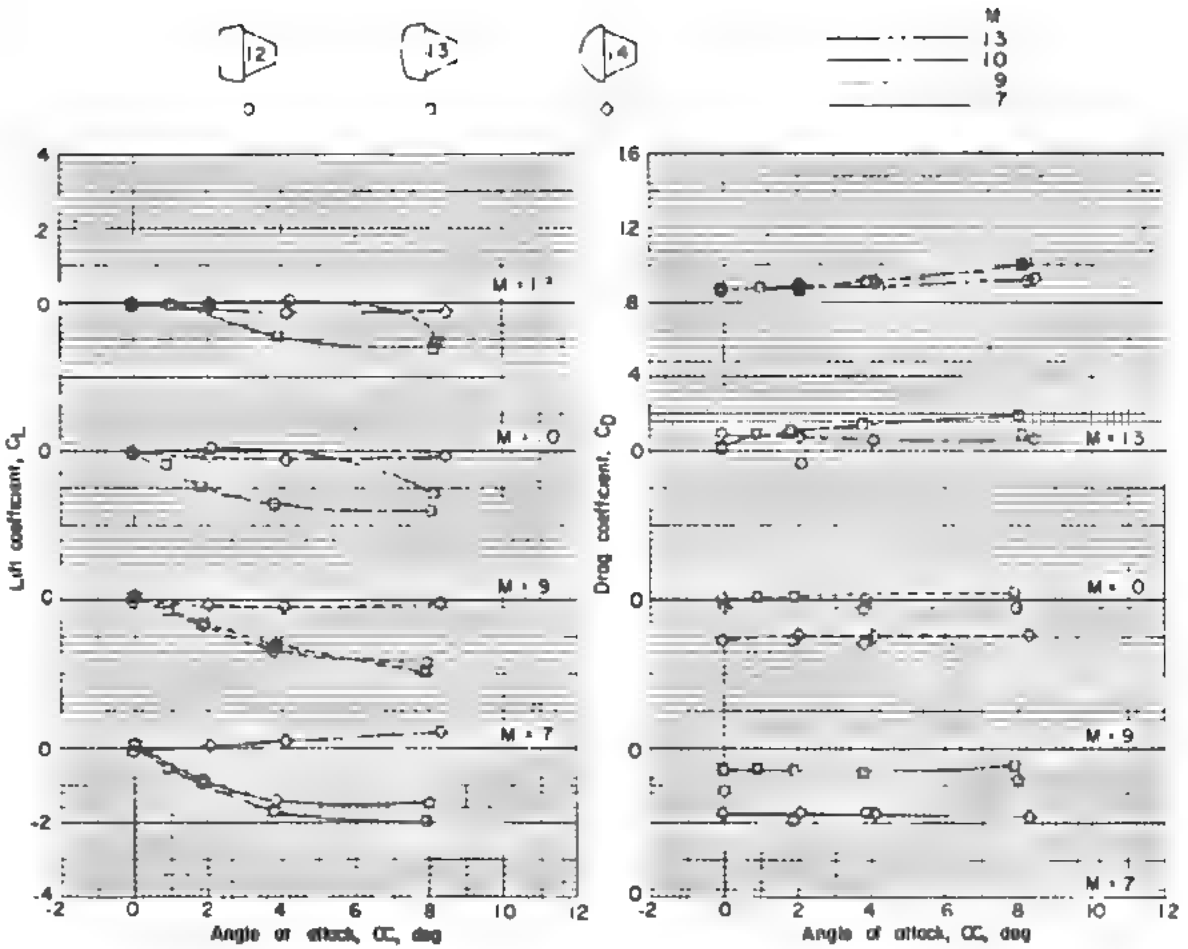

(a) Lift coefficient.

(b) Drag coefficient.

Figure 15.- Effect of nose curvature on the lift, drag, and pitching-moment coefficients for a family of blunt bodies; p_t = 70 psia.

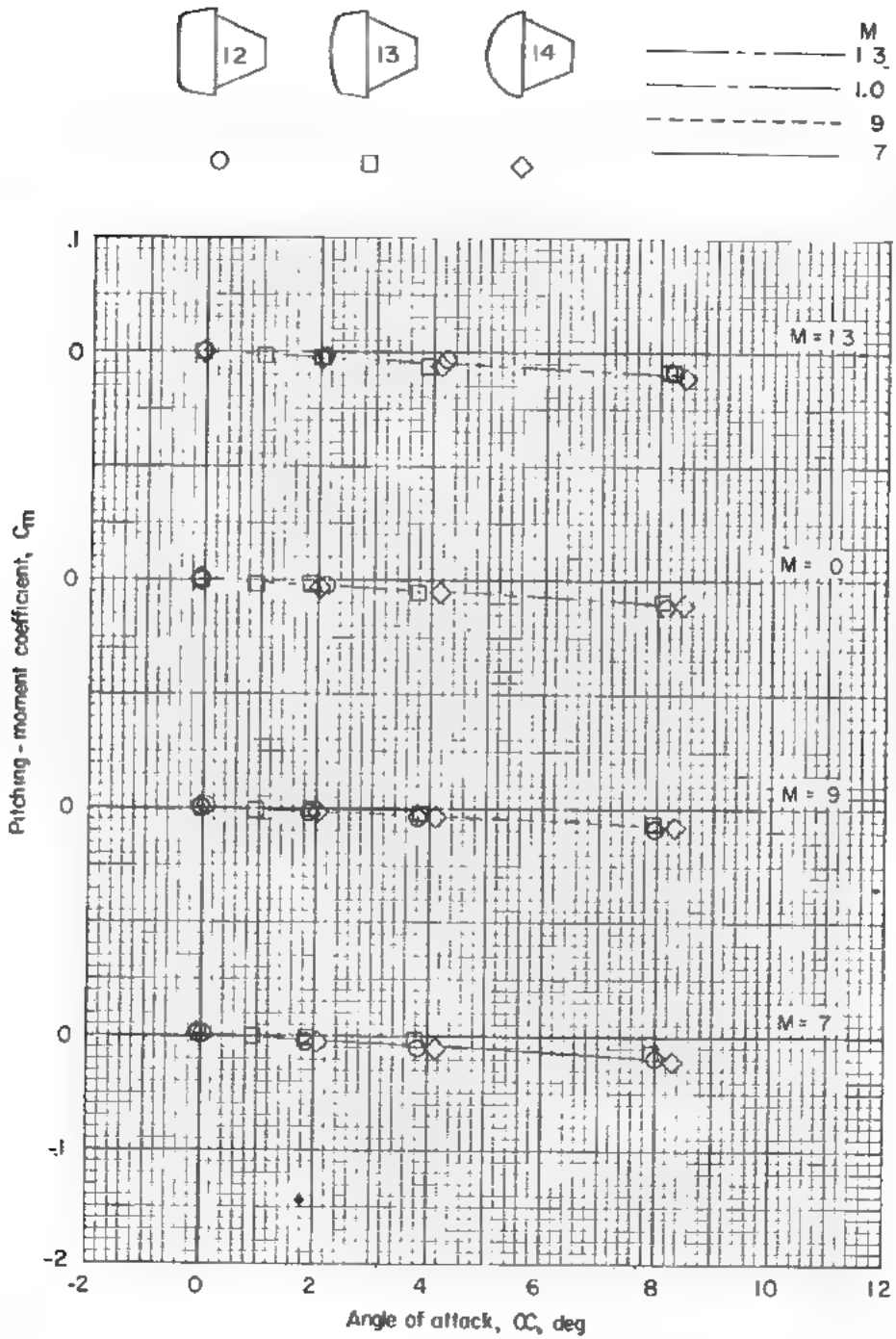

(c) Pitching-moment coefficient.

Figure 15.- Concluded.

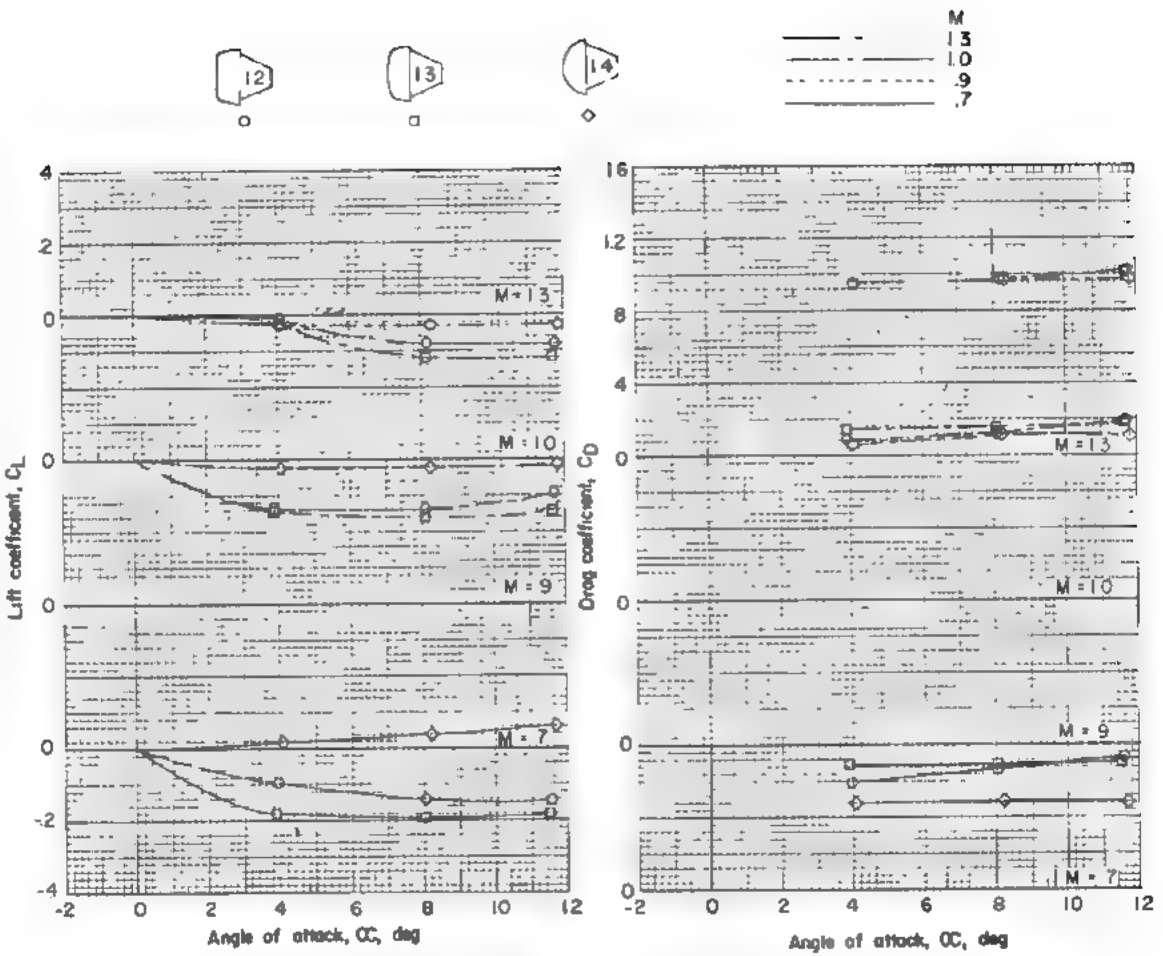

(a) Lift coefficient.

(b) Drag coefficient.

Figure 16.- Effect of nose curvature on the lift, drag, and pitching-moment coefficients for a family of blunt bodies; p_t = 35 psia.

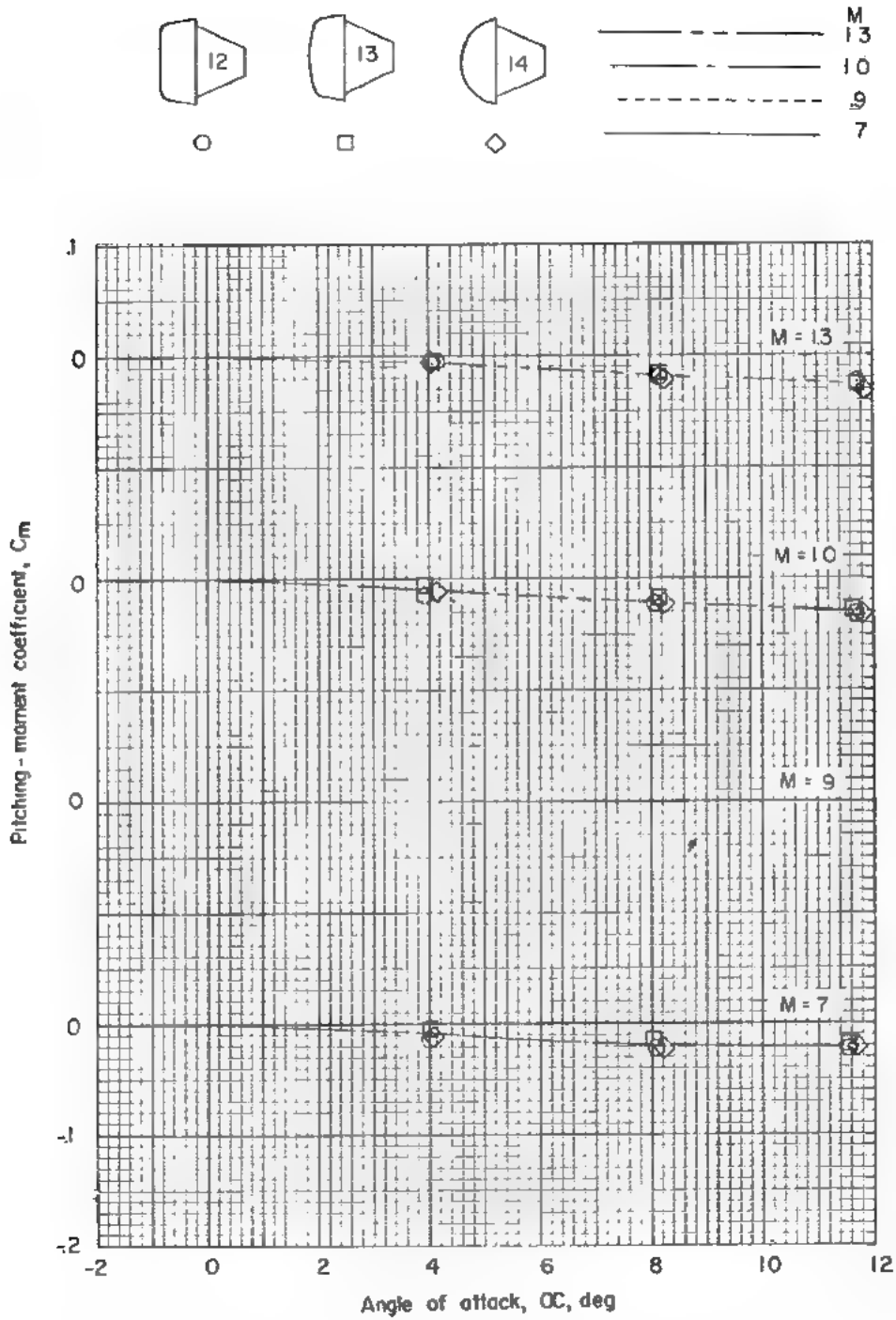

(c) Pitching-moment coefficient.

Figure 16.- Concluded.

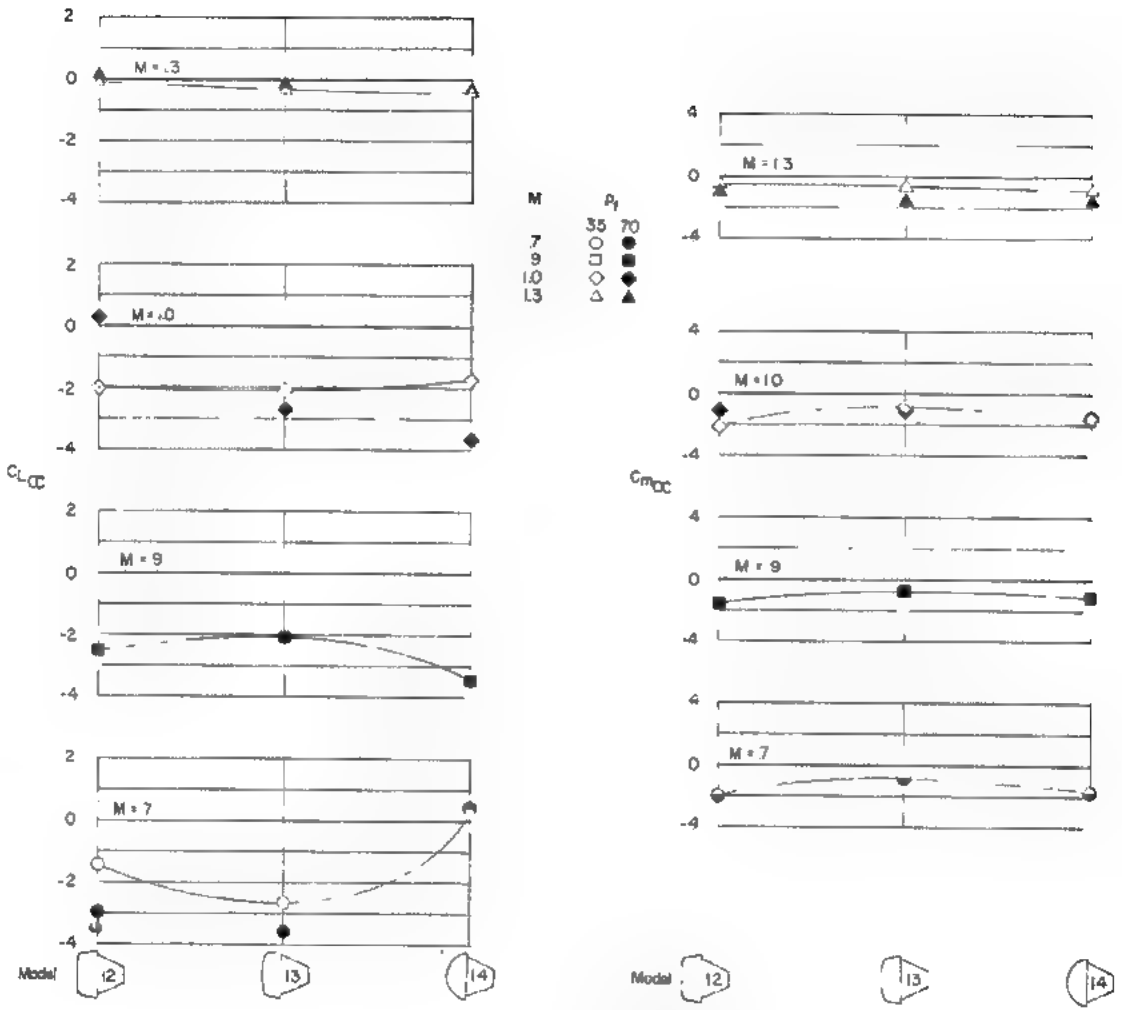

Figure 17.- Effect of nose curvature on the longitudinal stability derivatives for a family of blunt bodies.

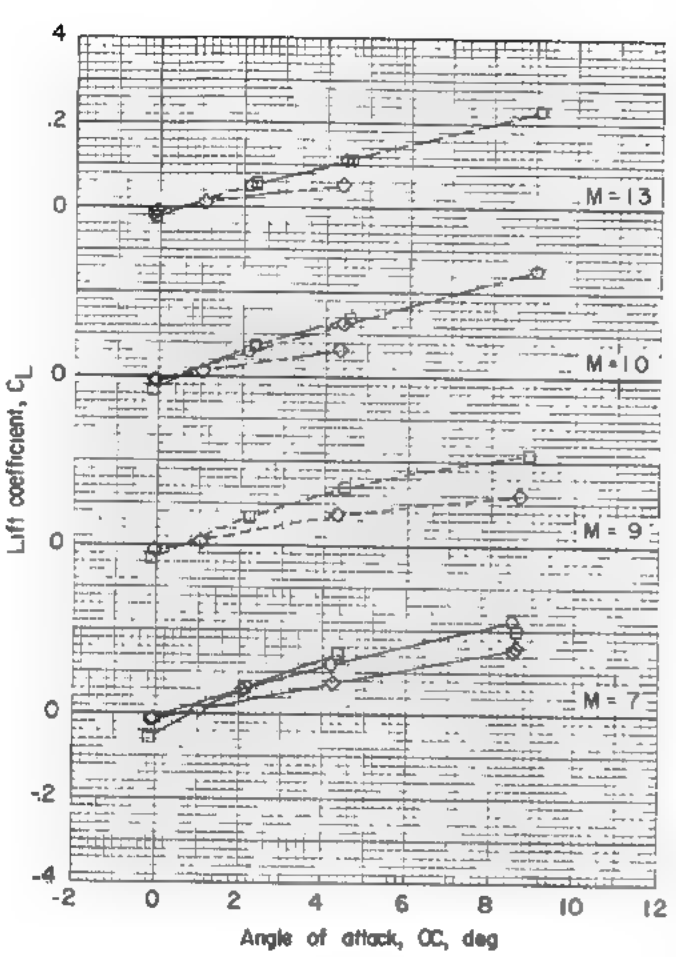

(a) Lift coefficient.

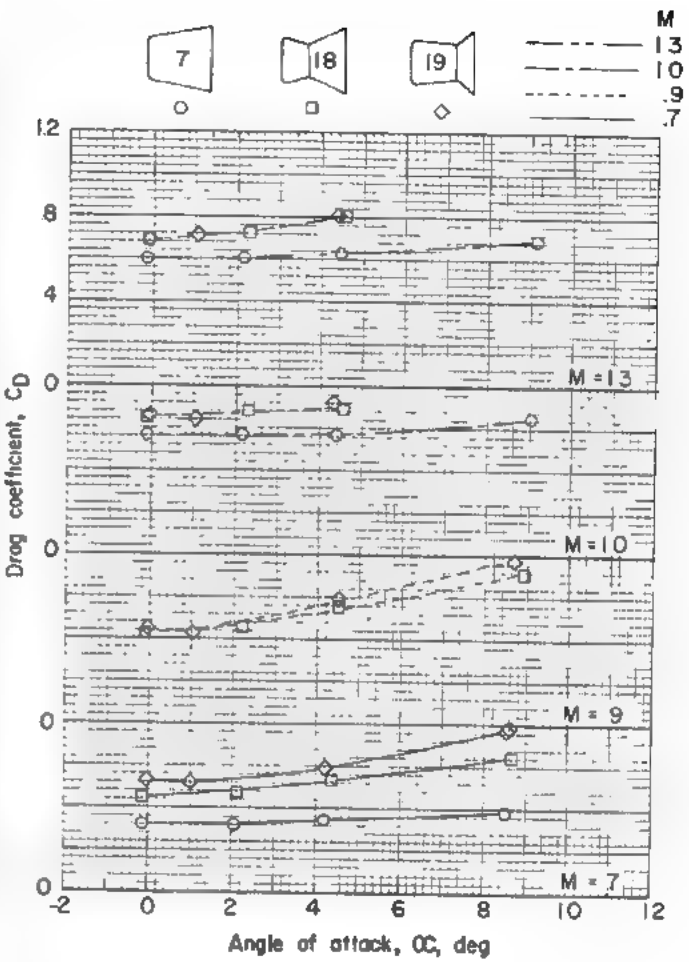

(b) Drag coefficient.

Figure 18.- Effect of body indentation on the lift, drag, and pitching-moment coefficients for a family of blunt bodies; p_t = 70 psia.

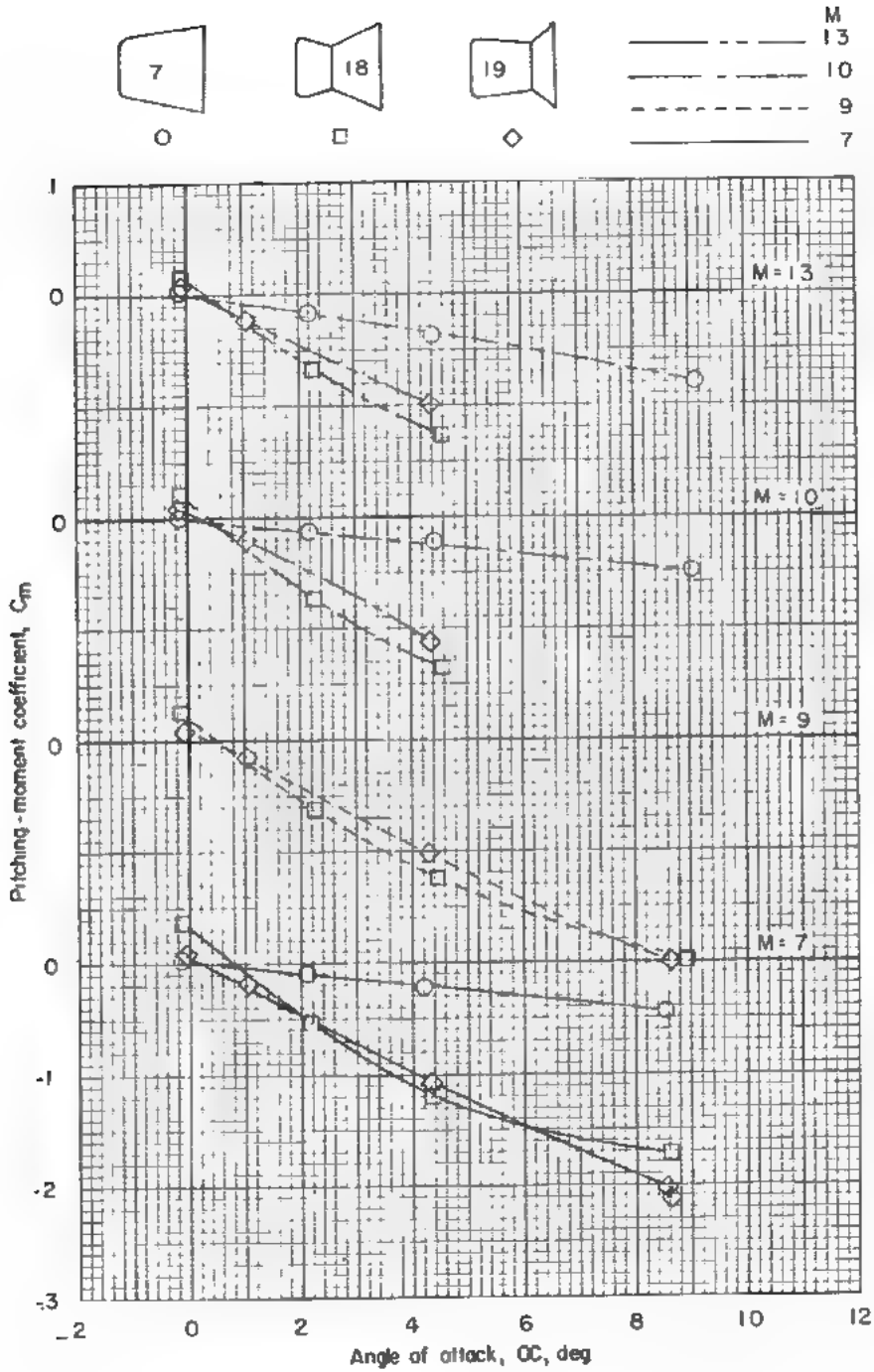

(c) Pitching-moment coefficient.

Figure 18.- Concluded.

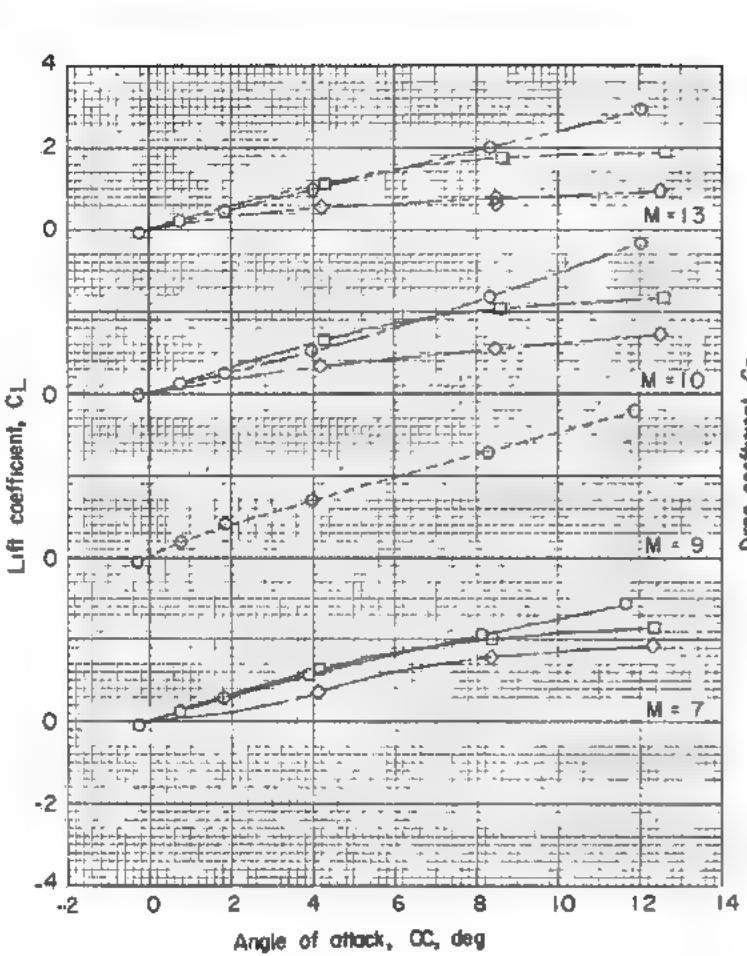

(a) Lift coefficient.

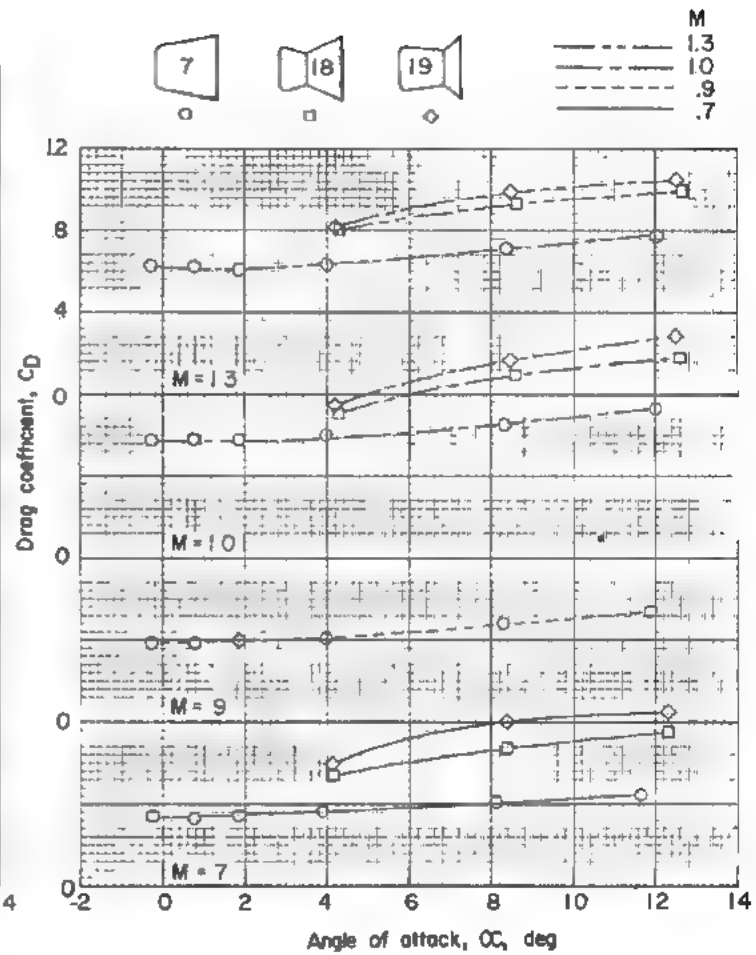

(b) Drag coefficient.

Figure 19.- Effect of body indentation on the lift, drag, and pitching-moment coefficients for a family of blunt bodies (models 7, 18, and 19); p_t = 35 psia.

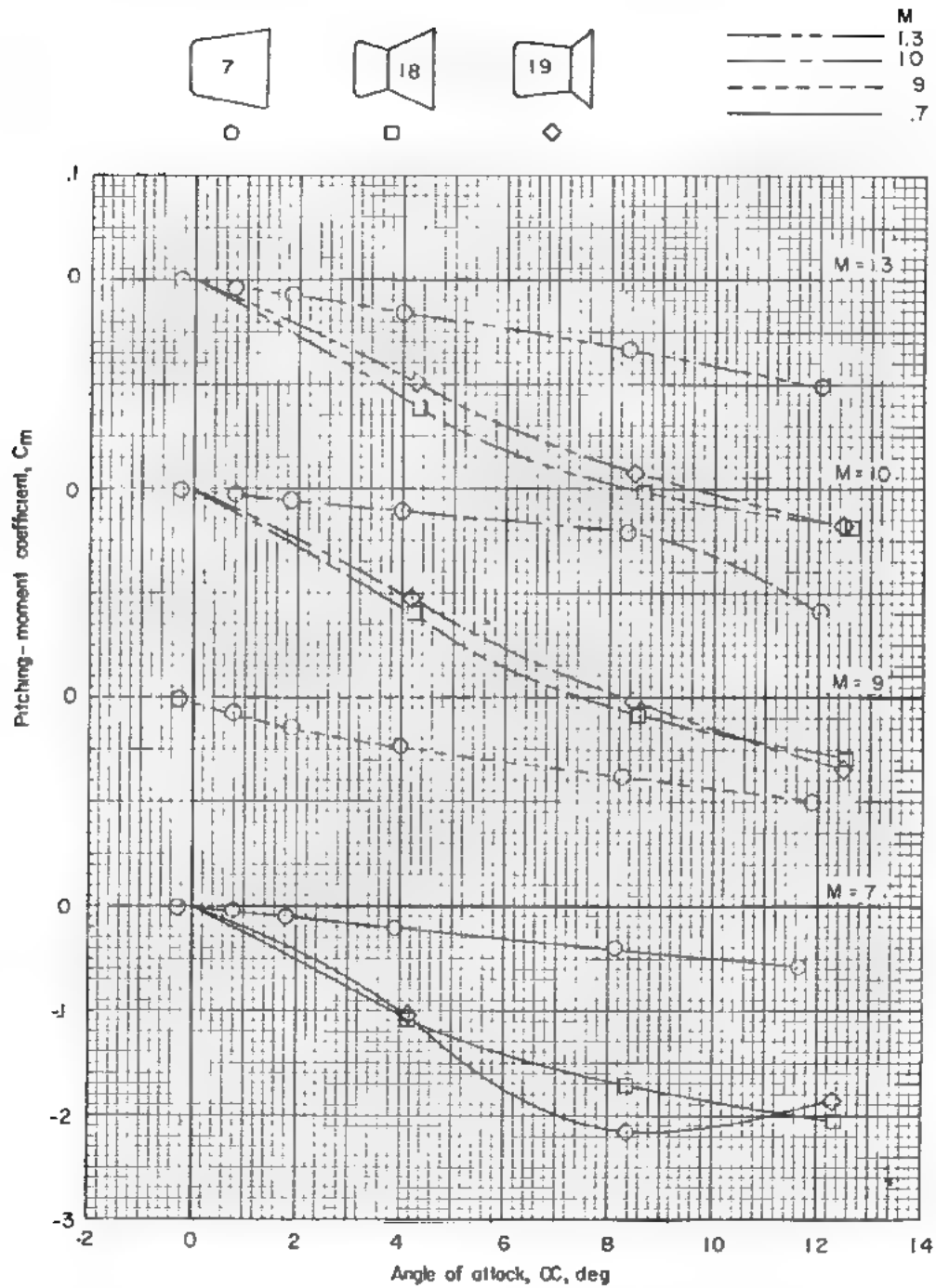

(c) Pitching-moment coefficient.

Figure 19.- Concluded.

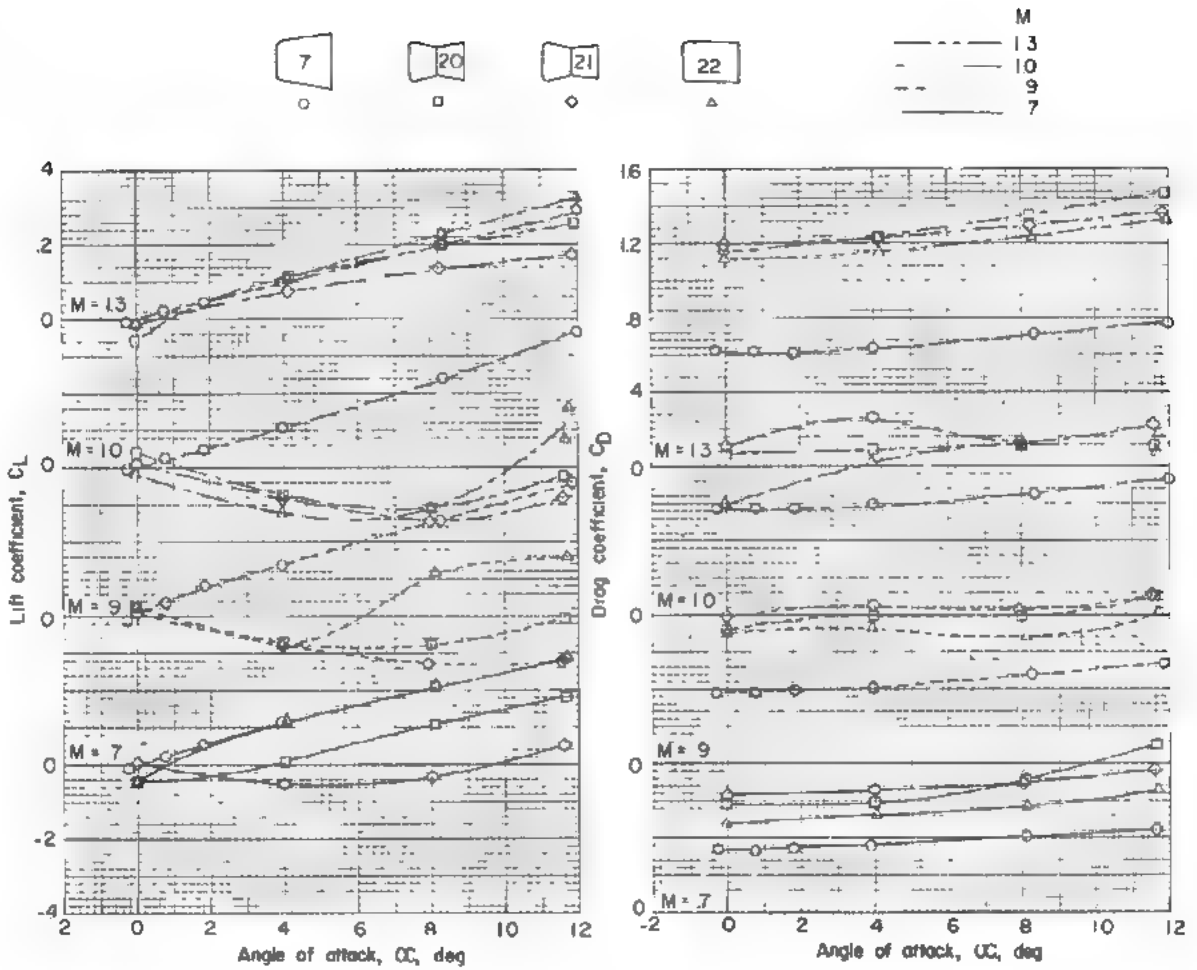

(a) Lift coefficient.

(b) Drag coefficient.

Figure 20.- Effect of body indentation on the lift, drag, and pitching-moment coefficients for a family of blunt bodies (models 7, 20, 21, and 22); p_t = 35 psia.

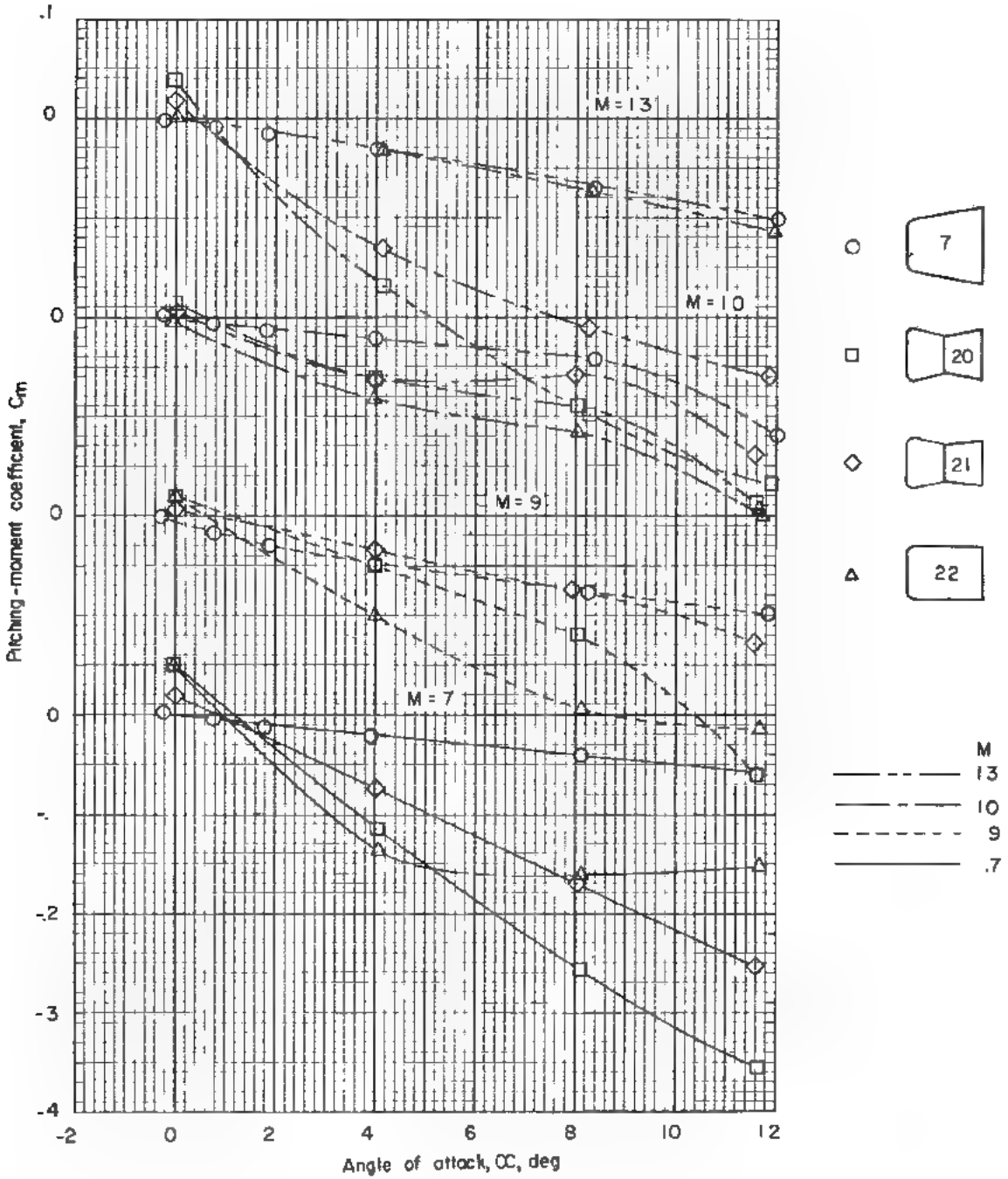

(c) Pitching-moment coefficient.

Figure 20.- Concluded.

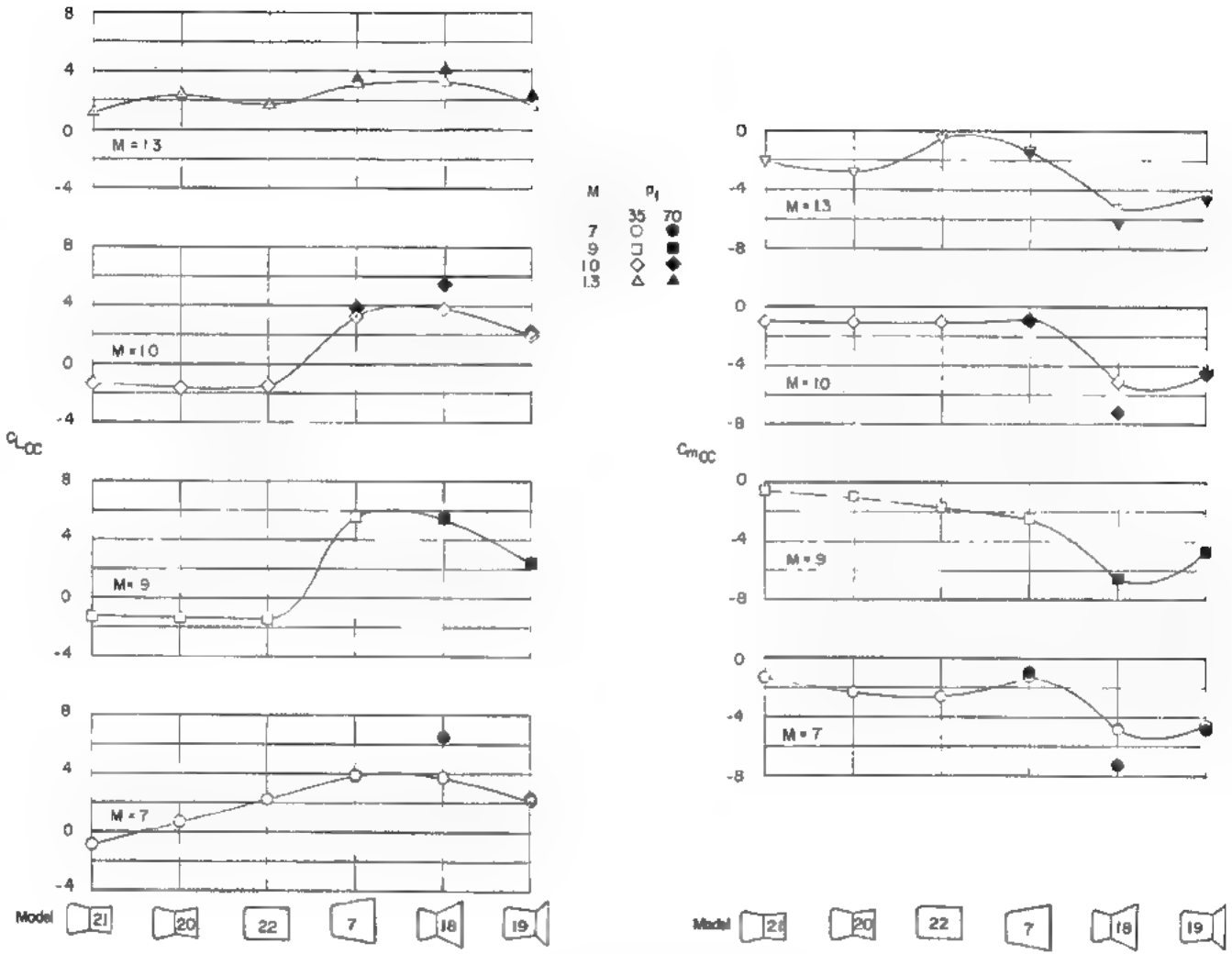

Figure 21.- Effect of body indentation on the longitudinal stability derivatives for a family of blunt bodies.

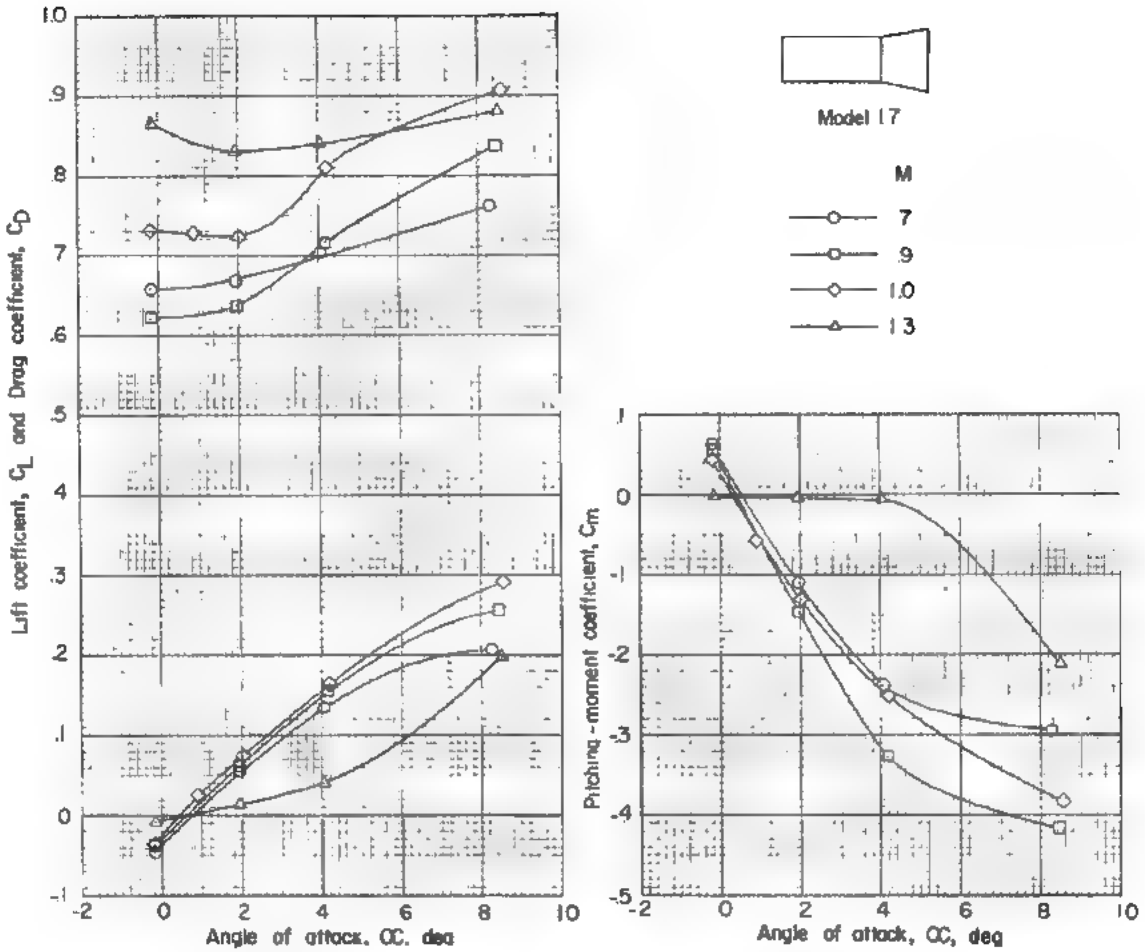

(a) Lift and drag coefficient.

(b) Pitching-moment coefficient.

Figure 22.- Lift, drag, and pitching-moment coefficients for a flared cylinder at transonic speeds; p_t = 35 psia; x_{cp}/l = 0.303.

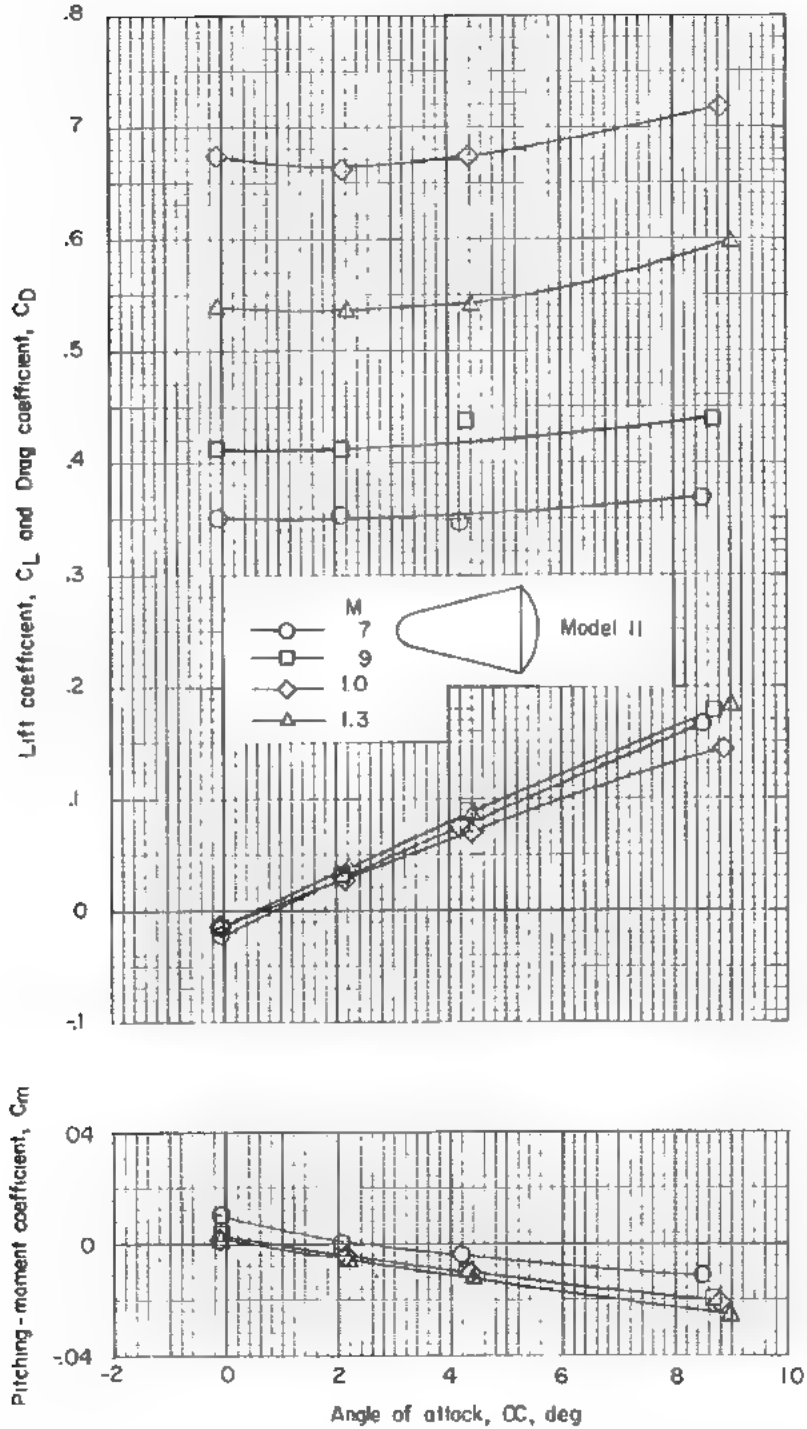

Figure 23.- Lift, drag, and pitching-moment coefficients for a round-nose cone at transonic speeds; p_t = 70 psia; x_{cp}/l = 0.580.

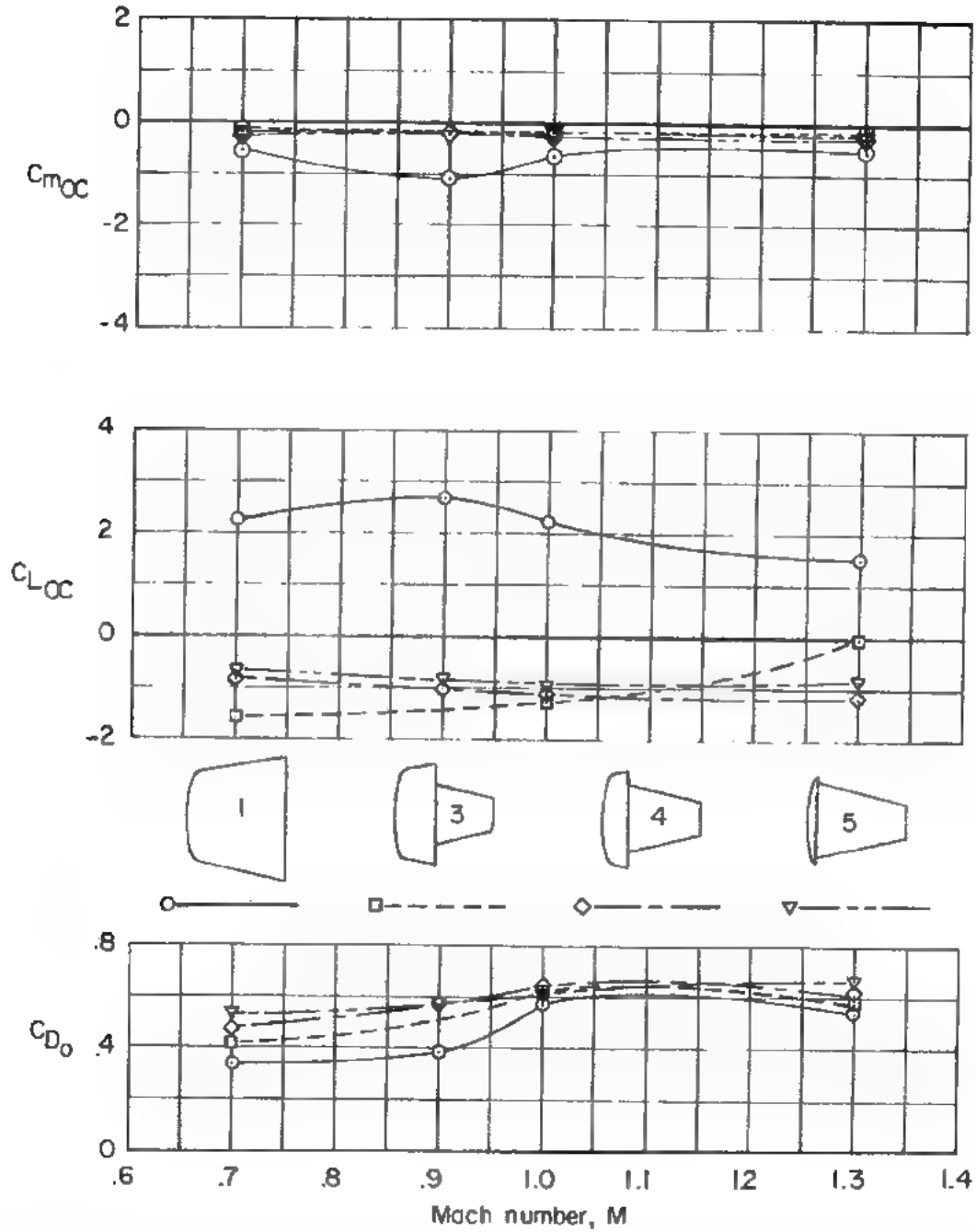

Figure 24.- Effect of Mach number on the aerodynamic coefficients for the skirt-length family of blunt shapes. All coefficients are based on maximum diameter of model 1. p_t = 70 psia for models 1, 3, 4; p_t = 35 psia for model 5.

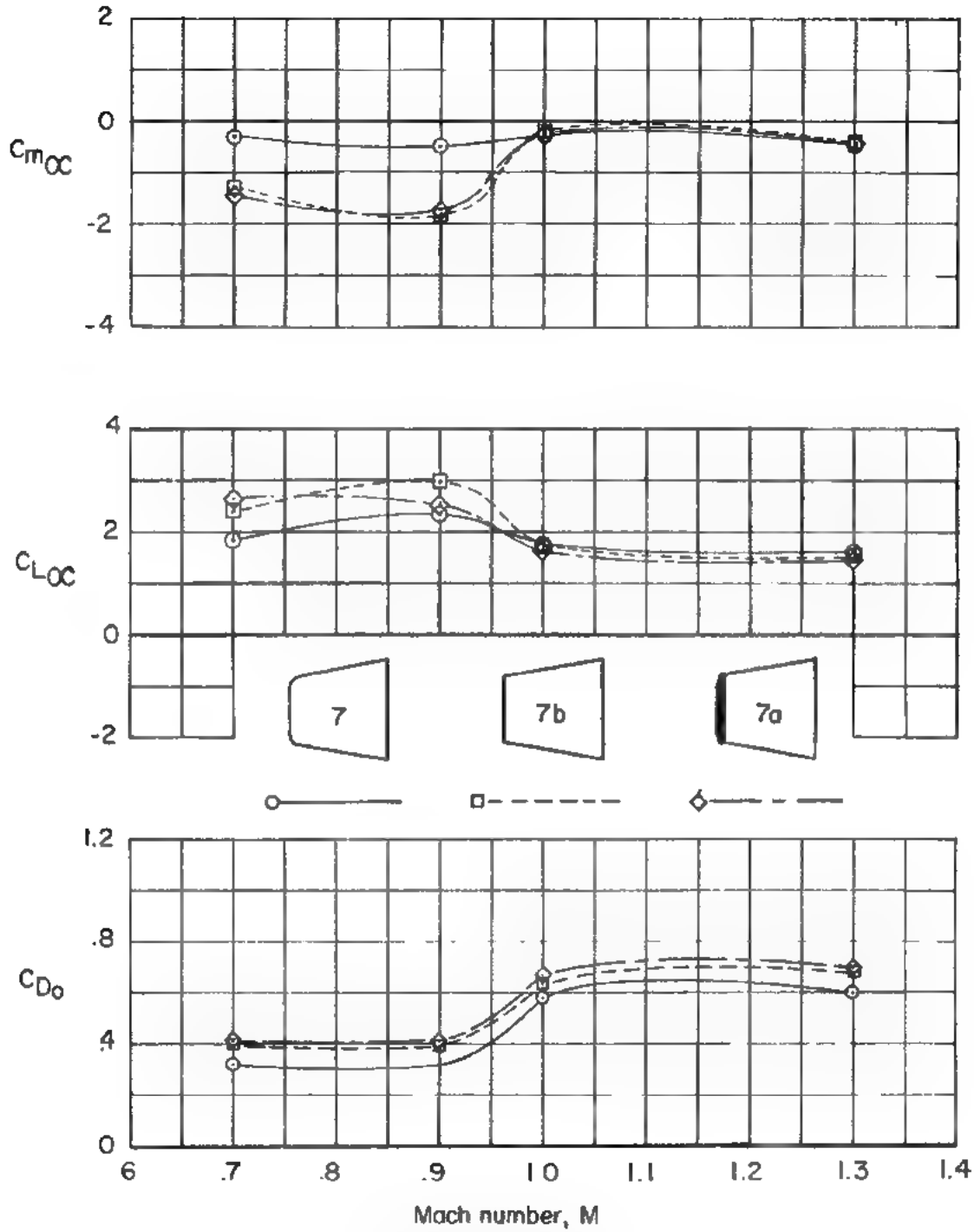

Figure 25.- Effect of Mach number on the aerodynamic coefficients for the shoulder-radius family of blunt bodies; p_t = 70 psia.

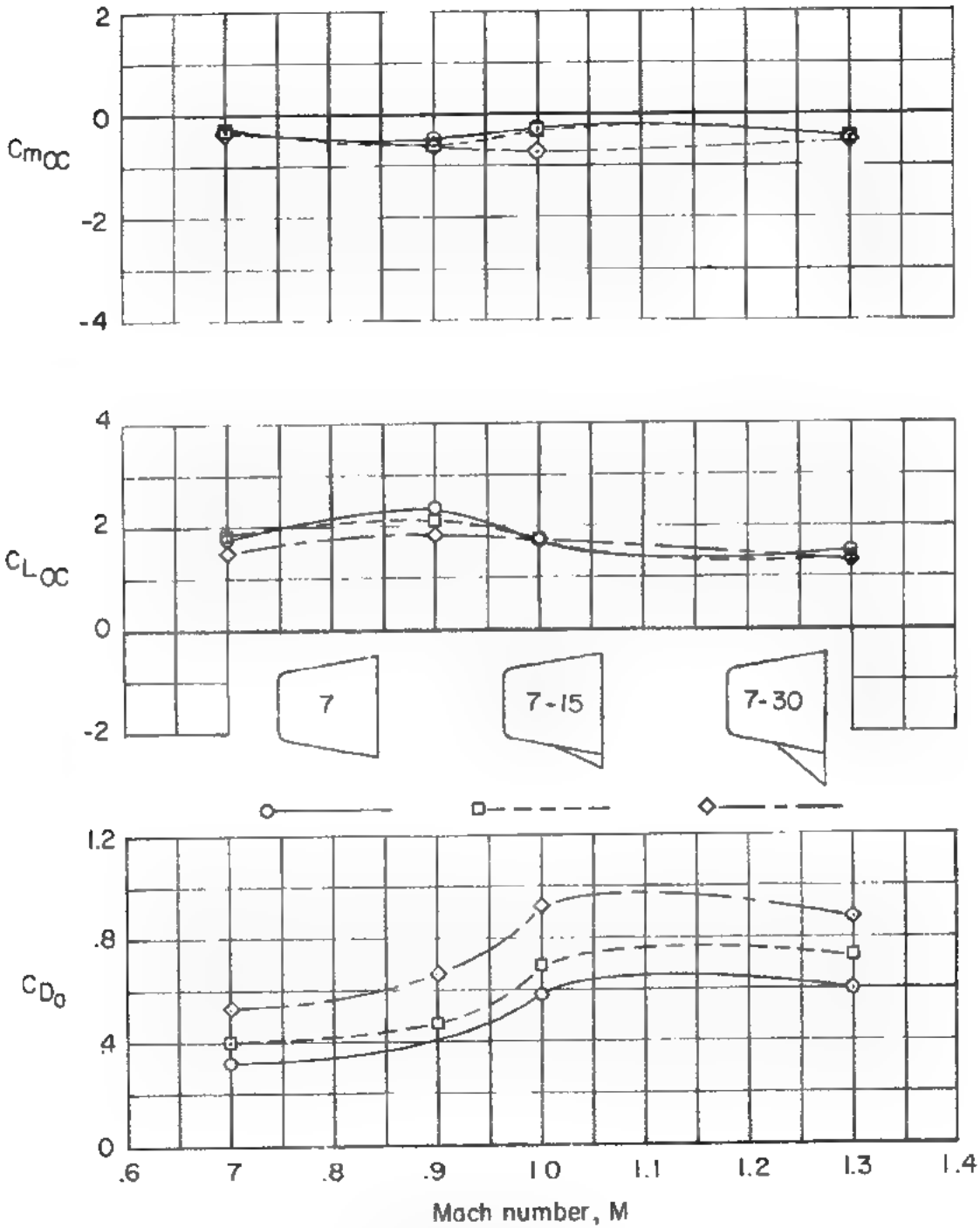

Figure 26.- Effect of Mach number on the aerodynamic coefficients for the control-wedge family of blunt bodies; p_t = 70 psia.

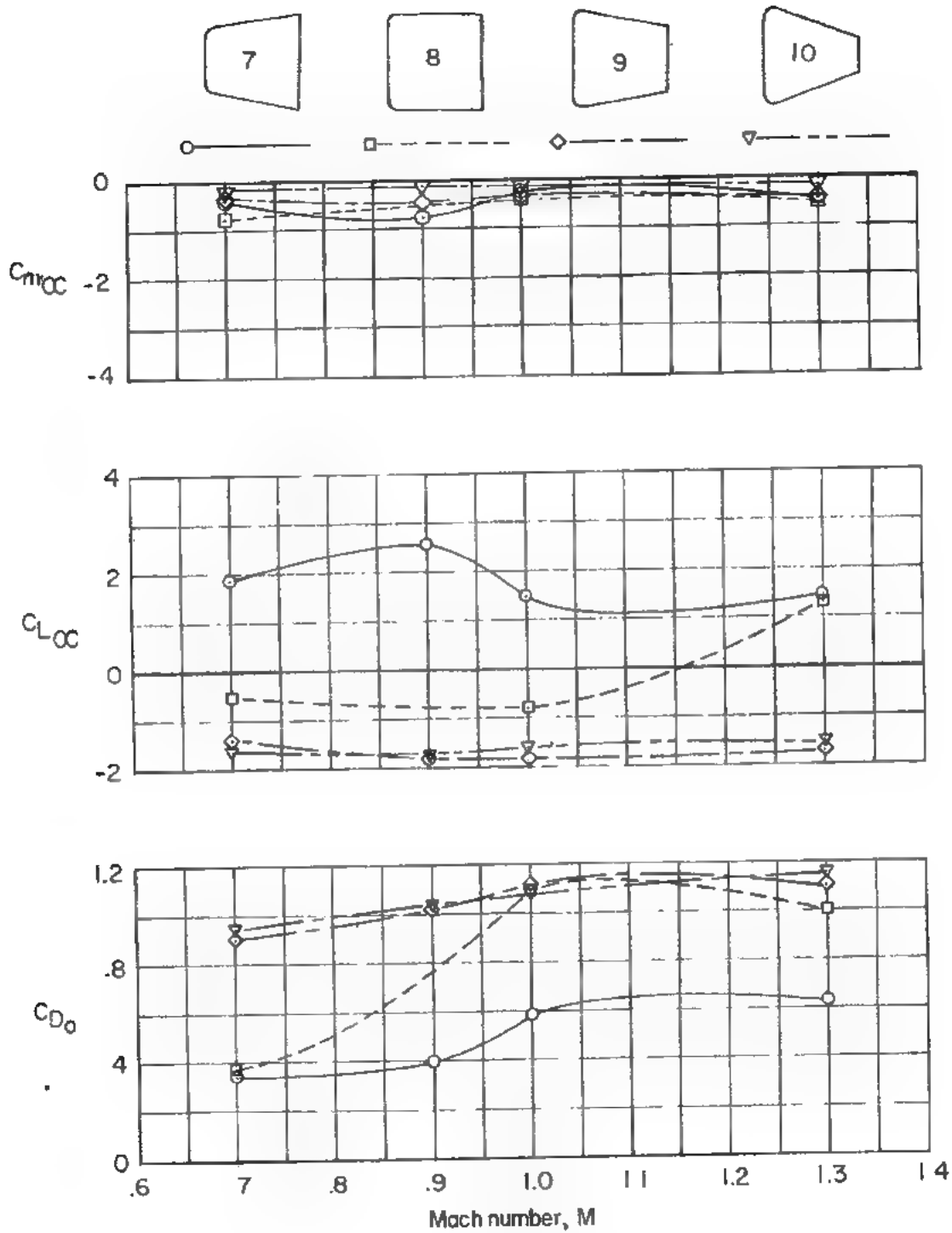

Figure 27.- Effect of Mach number on the aerodynamic coefficients for the body-slope family of blunt bodies; p_t = 35 psia.

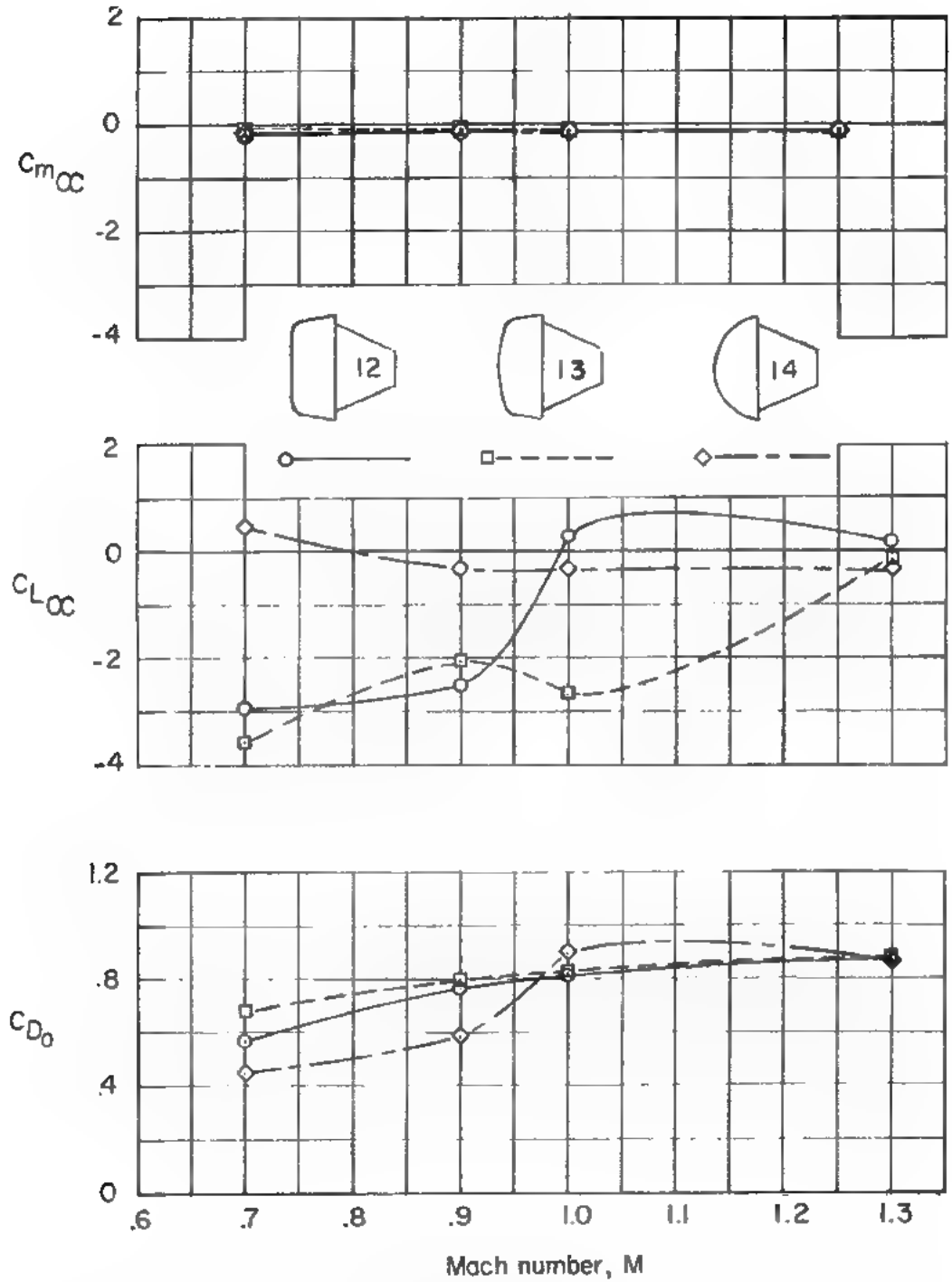

Figure 28.- Effect of Mach number on the aerodynamic coefficients for the nose-curvature family of blunt bodies; p_t = 70 psia.

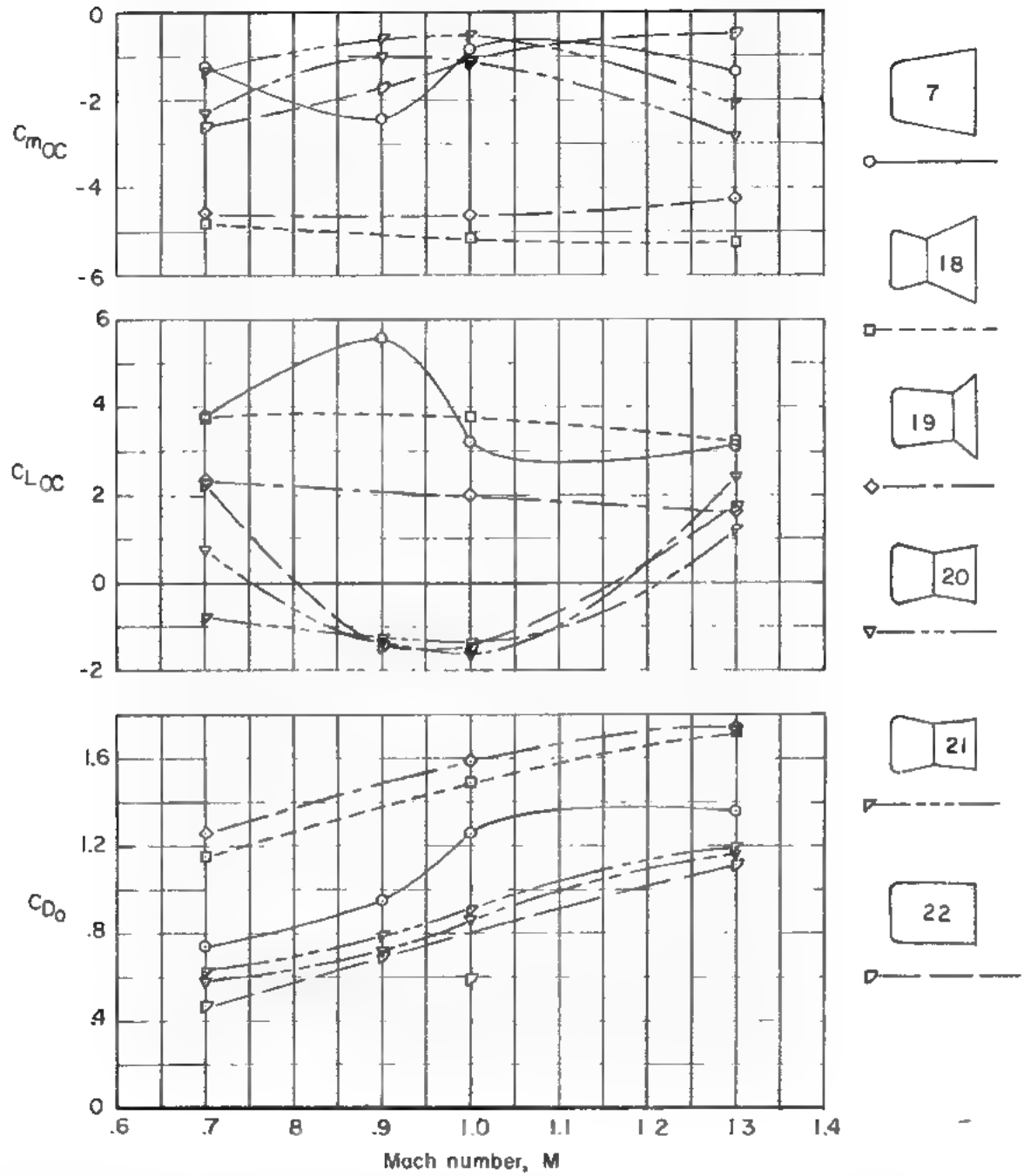

Figure 29.- Effect of Mach number on the aerodynamic coefficients for the indented-body family of blunt bodies. All coefficients based on maximum diameter of model 20; p_t = 35 psia.

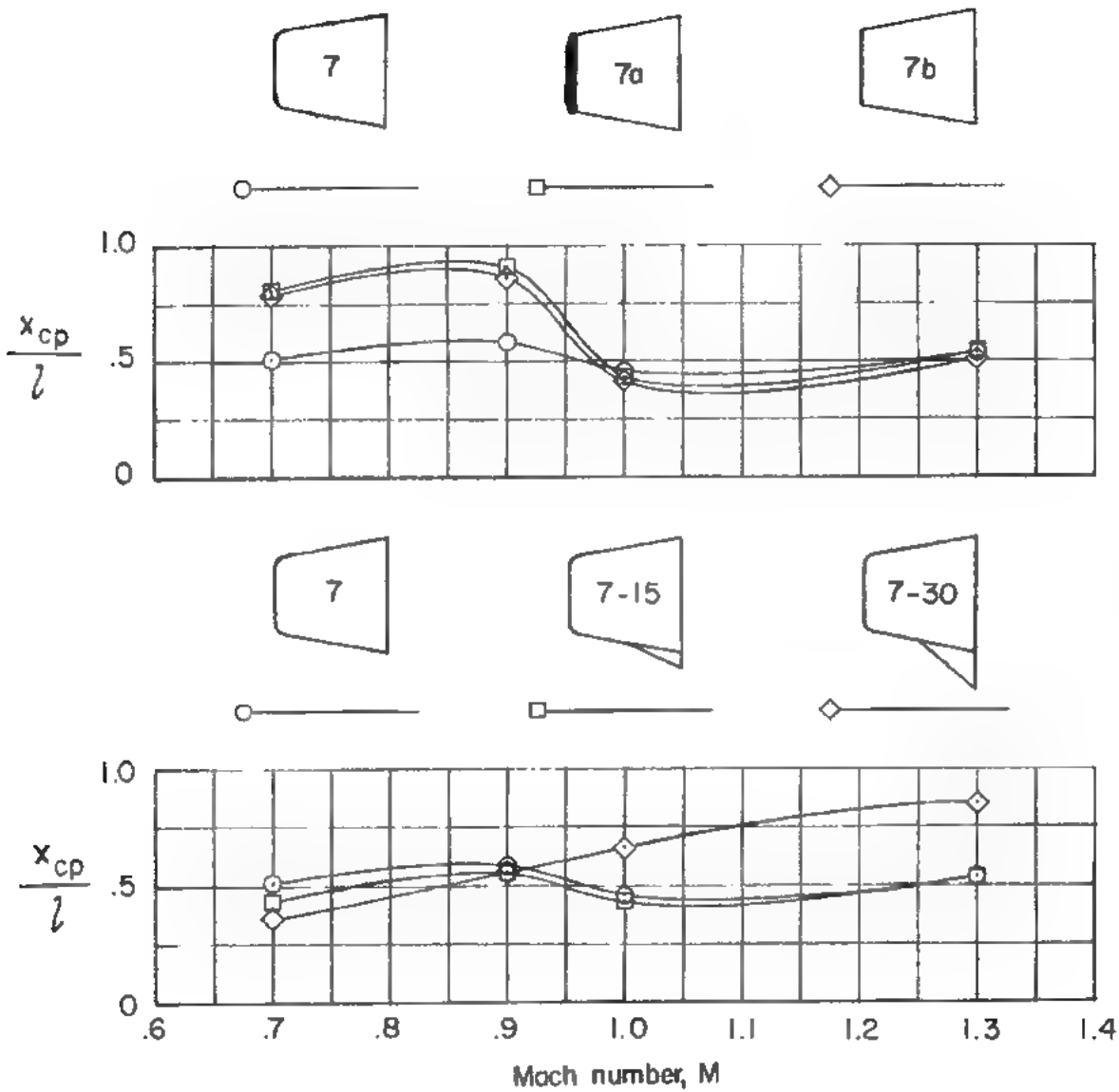

(a) Shoulder-radius and control-wedge families.

Figure 30.- Effect of Mach number on the center-of-pressure location for several families of blunt bodies.

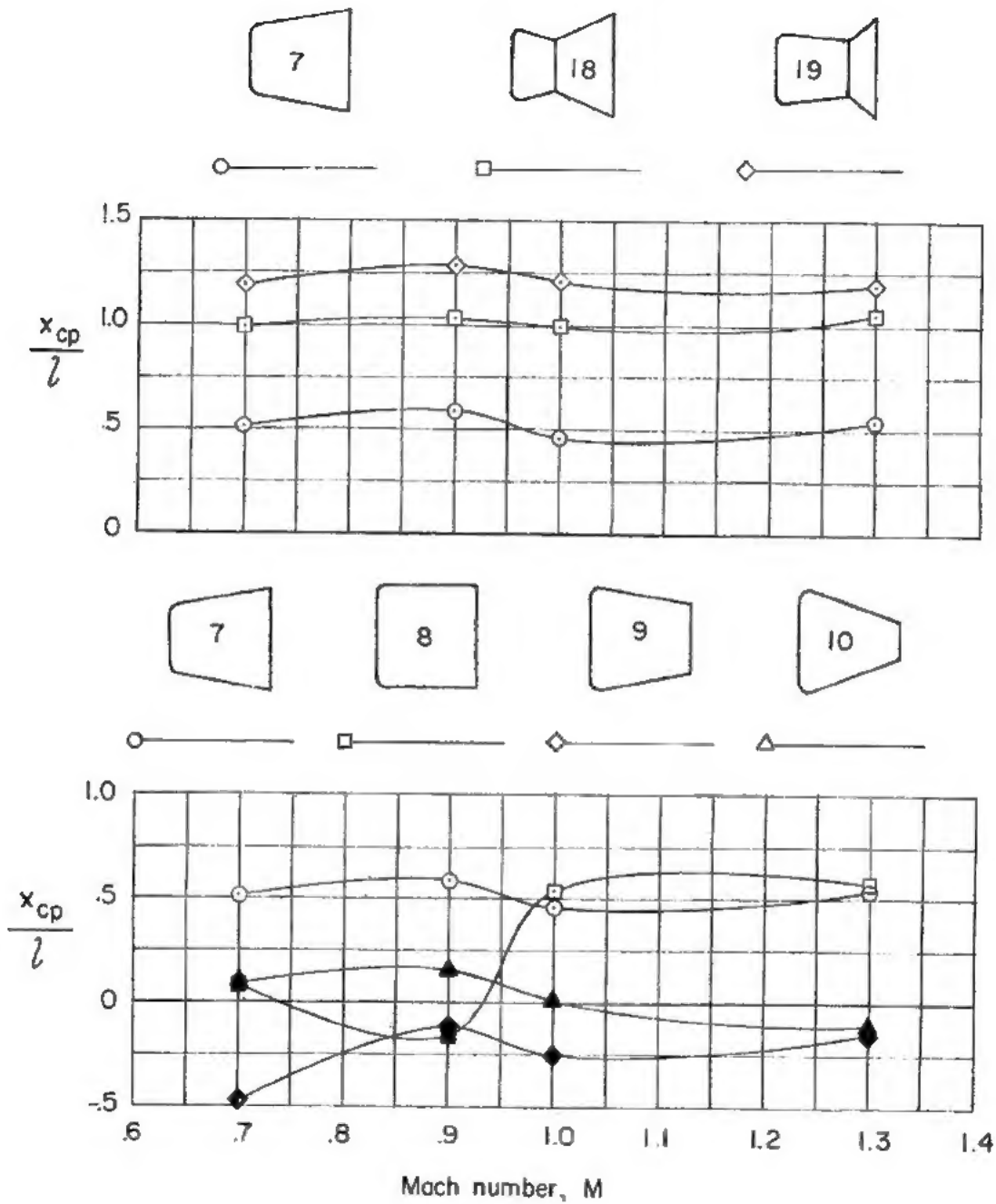

(b) Body-indentation and body-slope families. Solid symbols represent models for which lift-curve slope is negative.

Figure 30.- Continued.

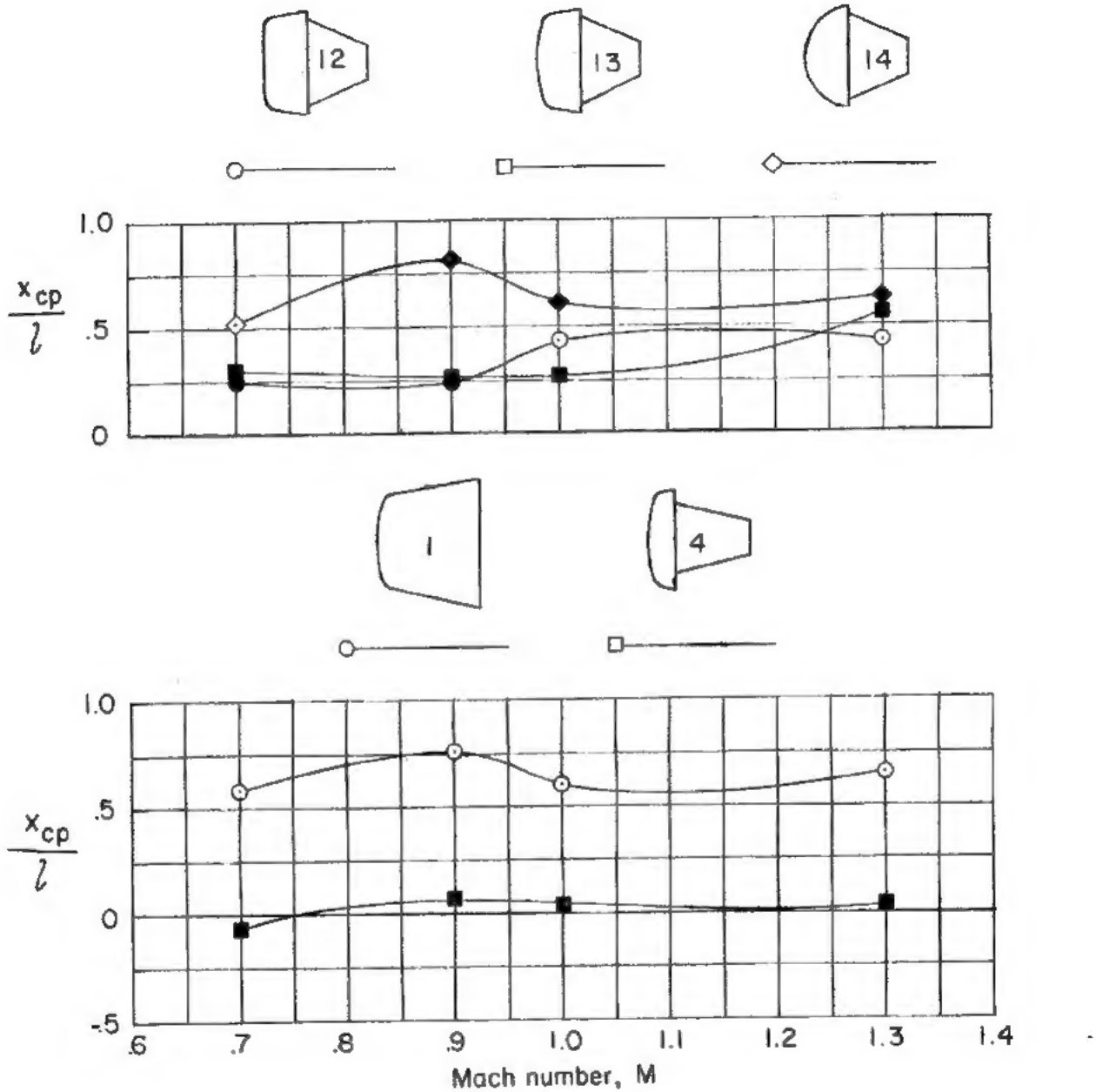

(c) Nose-curvature and skirt-length families. Solid symbols represent models for which lift-curve slope is negative.

Figure 30.- Concluded.

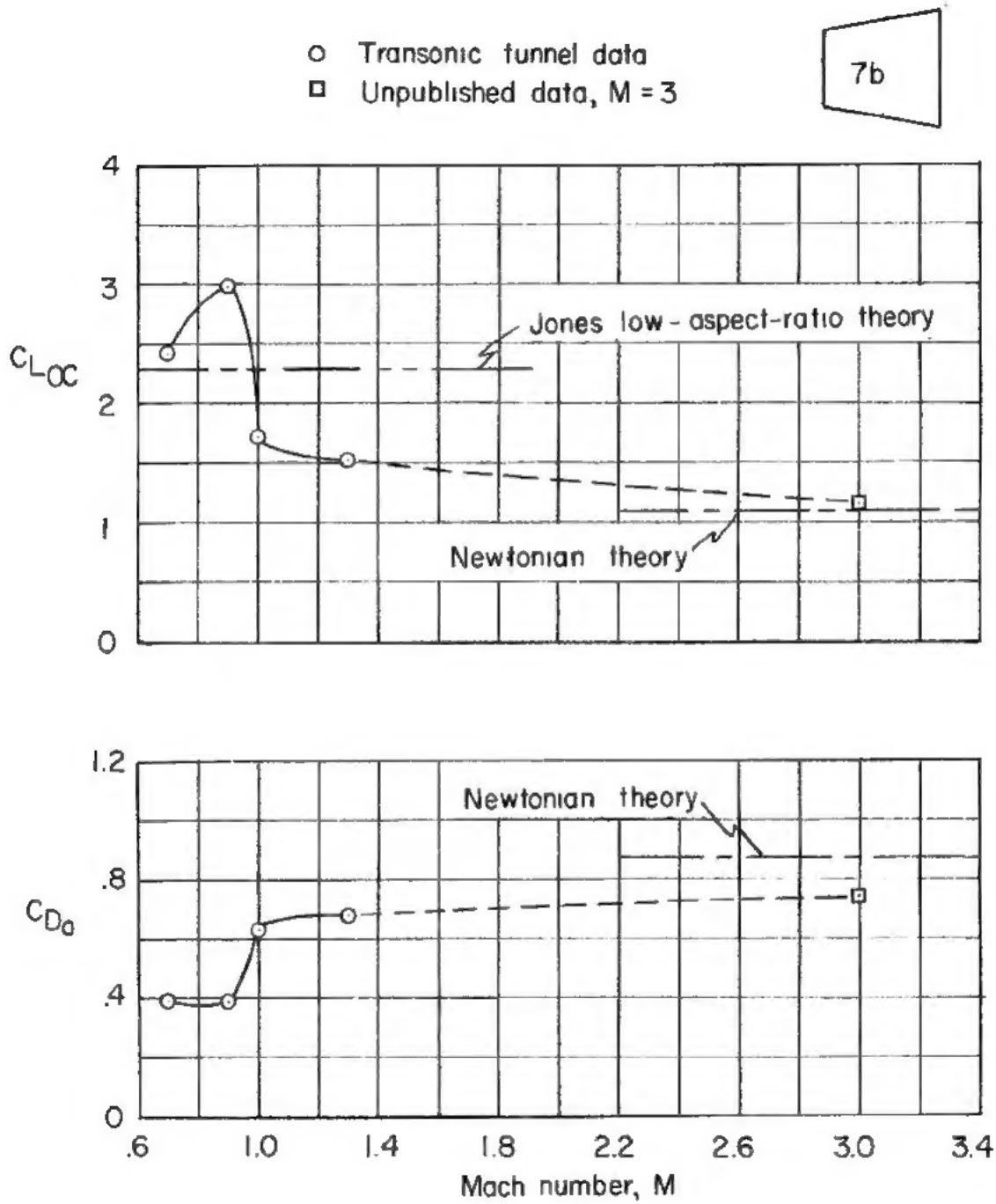

Figure 31.- Some comparisons of the test data with theoretical values for model 7b.